α_{1A}-adrenoceptor inverse agonists and agonists modulate receptor signalling through a conformational selection mechanism

Feng-Jie Wu[1,2,3], Lisa M. Williams[3], Alaa Abdul-Ridha[3], Avanka Gunatilaka[3], Tasneem M. Vaid[1,2,3], Martina Kocan[3], Alice R. Whitehead[3], Michael D.W. Griffin[1,2], Ross A.D. Bathgate[1,3], Daniel J. Scott[1,3*], Paul R. Gooley[1,2*]

[1]Department of Biochemistry and Molecular Biology, University of Melbourne, Parkville, 3052, VIC, Australia.

[2]Bio21 Molecular Science and Biotechnology Institute, University of Melbourne, Parkville, 3052, VIC, Australia.

[3]The Florey Institute of Neuroscience and Mental Health, University of Melbourne, Parkville, 3052, VIC, Australia.

Correspondence to:
Paul R. Gooley
Department of Biochemistry and Molecular Biology
The University of Melbourne
Bio21 Molecular Science and Biotechnology Institute
Phone: +61 (0)3 8344 2273
Email: prg@unimelb.edu.au

Daniel J. Scott
The Florey Institute of Neuroscience and Mental Health
The University of Melbourne
Phone: +61 (0)3 9035 7584
Email: daniel.scott@florey.edu.au

Abstract

G-Protein Coupled Receptors (GPCRs) transmit signals across the cell membrane via an allosteric network from the ligand-binding site to the G-protein binding site via a series of conserved microswitches. Crystal structures of GPCRs provide snapshots of inactive and active states, but poorly describe the conformational dynamics of the allosteric network that underlies GPCR activation. Here we analyse the correlation between ligand binding and receptor conformation of the α_{1A}-adrenoceptor, known for stimulating smooth muscle contraction in response to binding noradrenaline. NMR of $^{13}C^{\varepsilon}H_3$-methionine labelled α_{1A}-adrenoreceptor mutants, each exhibiting differing signalling capacities, revealed how different classes of ligands modulate receptor conformational equilibria. $^{13}C^{\varepsilon}H_3$-methionine residues near the microswitches revealed distinct states that correlated with ligand efficacies, supporting a conformational selection mechanism. We propose that allosteric coupling between the microswitches controls receptor conformation and underlies the mechanism of ligand modulation of GPCR signalling in cells.

Introduction

G-protein coupled receptors (GPCRs) are integral membrane proteins sharing a common seven-helix transmembrane domain (TMD). Conformational changes to the TMD are required to transmit the extracellular stimuli intracellularly to activate signalling pathways. Over the past 20 years X-ray crystal structures, and more recently cryo-EM structures, have revealed a plethora of structural details on how functionally different ligands interact with GPCRs and the conformational changes they induce. Most structures solved to date are of GPCRs in inactive states, bound to inverse agonists or antagonists (Manglik and Kruse, 2017). A few have been crystalized with agonist alone (Manglik and Kruse, 2017), with resultant structures similar to antagonist bound inactive states. Complexes of GPCRs with active-state-stabilising nanobodies, engineered mini G proteins, Gα C-terminal peptide or heterotrimeric G proteins appear necessary to stabilise agonist bound GPCRs in active states for X-ray and cryo-EM structure determination (Carpenter and Tate, 2017). Using these tools, several active state GPCR structures have been solved (Carpenter and Tate, 2017; Garcia-Nafria and Tate, 2019; Manglik and Kruse, 2017), revealing conserved conformational changes that occur upon receptor activation. These include rearrangements in the ligand binding site and a large outward movement at the cytoplasmic side of transmembrane (TM) helix 6 (TM6) to accommodate G protein binding. While providing a wealth of structural detail of static receptor conformations, these structures generally do not provide insight into GPCR signalling complexities such as basal receptor activity, partial agonism and biased agonism.

To address this shortfall, spectroscopic techniques, supported by molecular dynamic simulations, have given insight into the conformational dynamics that underlie the activity of a few diffusible ligand-activated GPCRs including β_2 adrenergic receptor (β_2-AR) (Bokoch

et al., 2010; Eddy et al., 2016; Horst et al., 2013; Kofuku et al., 2012; Kofuku et al., 2014; Liu, 2012; Manglik et al., 2015; Nygaard et al., 2013), β_1 adrenergic receptor (β_1-AR) (Isogai et al., 2016; Solt et al., 2017), adenosine A_{2A} receptor ($A_{2A}R$) (Clark et al., 2017; Eddy et al., 2018; Ye et al., 2018; Ye et al., 2016), μ opioid receptor (μOR) (Okude et al., 2015; Sounier et al., 2015), leukotriene B4 receptor (BLT2)(Casiraghi et al., 2016), and the M2 muscarinic acetylcholine receptor (M2R) (Xu et al., 2019). By far the most studied receptor in this regard is β_2-AR, for which $^{13}C^{\varepsilon}H_3$-methionine labelling NMR (Bokoch et al., 2010; Kofuku et al., 2012; Kofuku et al., 2014; Nygaard et al., 2013), ^{19}F NMR(Eddy et al., 2016; Horst et al., 2013; Liu, 2012; Manglik et al., 2015) and electron paramagnetic resonance (EPR) (Manglik et al., 2015) have been applied to characterise the conformational signatures of this receptor when bound to various ligands and a G protein mimetic nanobody. These studies reveal that GPCRs are highly dynamic, sampling inactive and active conformational states, and are thought to predominantly function via a conformational selection mechanism (Shimada et al., 2018). Such a mechanism posits that a GPCR constantly samples various inactive and active conformations, all existing in equilibrium. Ligands preferentially bind to particular receptor states, depending on their pharmacological characteristics, thus shifting the conformational equilibrium towards these preferred states and modulating the signalling output of the system. The extracellular orthosteric ligand binding site in adrenoceptors is connected to the intracellular G protein binding site through a series of conserved microswitches (Ahuja and Smith, 2009; Deupi and Standfuss, 2011; Trzaskowski et al., 2012) (Figure 1): a central transmission switch (also called the connector region, CWxP motif or PIF motif (Latorraca et al., 2017)), the NPxxY switch, and the intracellular G protein binding site, characterized by the DRY motif (or switch). How these microswitches coordinate the transmission of the extracellular signal is not clear, but molecular dynamics (MD) simulations and NMR data have led to a mechanistic description of "loose allosteric coupling" (Latorraca et al., 2017).

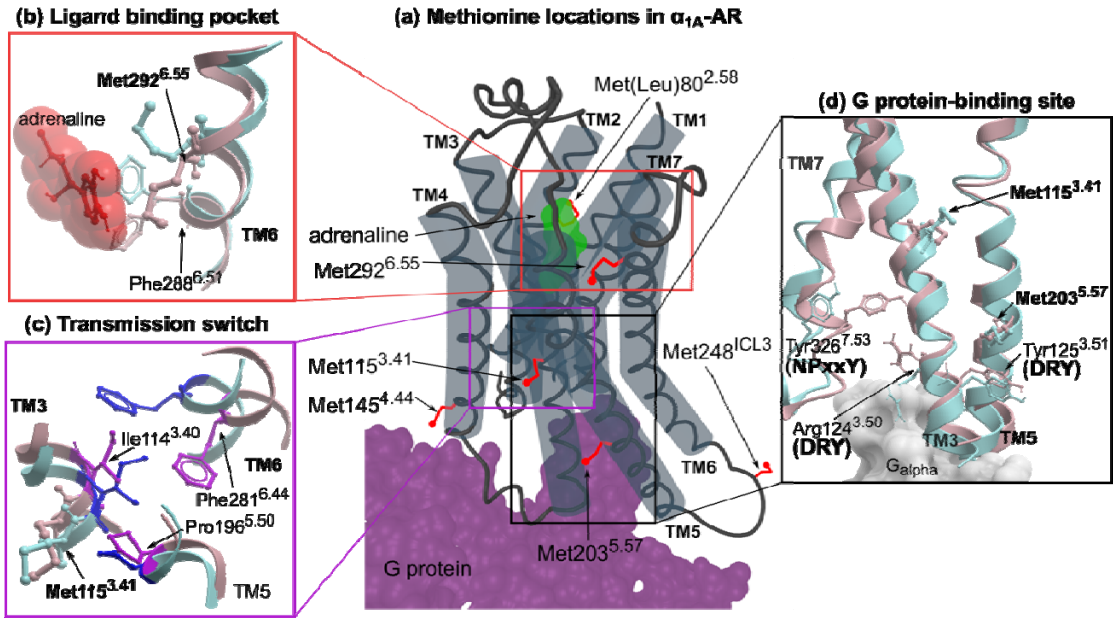

Figure 1. Methionine residues in α_{1A}-AR. (a) The location of six methionines on a cartoon representation of α_{1A}-AR. Methionine sidechains are highlighted as red sticks. Bound adrenaline and G protein are coloured in green and purple respectively. (b-d) Homology models of α_{1A}-AR-A4 in the inactive state (blue; modeled on the X-ray crystal structure of inactive β_2-AR, pdb id: 5jqh) and active state (pink; modeled on the X-ray crystal structure of active β_2-AR, pdb id: 3sn6) are superimposed showing inferred conformational changes that occur in the ligand binding pocket (b), transmission switch (c) and G protein binding site (d).

This mechanism refers to each microswitch as conformationally independent from the others, that is an active DRY motif state is not significantly dependent on an active state in the transmission switch. That said, an active state in the transmission switch does increase the probability of the DRY motif (and thus the receptor) to sample active states (thus, loose allosteric coupling) (Latorraca et al., 2017). Put simply, the conformational changes that occur in the microswitches are thought to drive the overall equilibrium state of the receptor

system. Despite recent work, it is not well understood how the binding of ligands such as inverse agonists influence the microswitch state equilibria to decrease basal receptor activity.

α_1-adrenoceptors (α_1-ARs) comprise three G_q-coupled GPCR subtypes (α_{1A}-, α_{1B}- and α_{1D}-AR) that bind and sense the endogenous catecholamines, adrenaline and noradrenaline, to modulate a range of physiological processes. In the periphery, postsynaptic α_1-AR stimulation by catecholamines mediates smooth muscle contraction, thus α_1-AR antagonists and inverse agonists are clinically prescribed to treat hypertension and benign prostatic hyperplasia (BPH) (Akinaga et al., 2019). α_1-ARs are also widely expressed in the central nervous system (CNS), but the lack of subtype-selective antibodies and ligands limits the understanding of their role in neuroplasticity and neurodegeneration (Perez and Doze, 2011). Currently there are no available crystal structures of an α_1-AR family member, which limits the rational design of more selective compounds to probe the physiological role of α_{1A}-AR in the CNS.

Recombinant α_{1A}-AR expresses poorly and the resultant protein is particularly unstable when purified in detergent (Scott and Pluckthun, 2013), which has hindered biochemical studies of this GPCR. Recently, we engineered an α_{1A}-AR variant, α_{1A}-AR-A4, that can be expressed in *Escherichia coli* (*E. coli*) and exhibits improved stability when purified in detergents (Yong et al., 2018). When expressed in COS-7 cells α_{1A}-AR-A4 exhibits no signalling efficacy in response to adrenaline stimulation (Yong et al., 2018). In the present study, α_{1A}-AR-A4 was labelled with $^{13}C^{\varepsilon}H_3$-methionine at the five naturally occurring methionine residues, providing NMR probes to assess how inverse agonists, partial agonists and full agonists influence receptor conformational equilibria. Three of these methionines are excellent probes of the ligand-binding site and the microswitches proposed to be markers of signal transmission: Met292$^{6.55}$ (superscript denotes GPCRdb numbering (Isberg et al., 2015)) is located in the ligand binding site; Met115$^{3.41}$ is proximal to the

transmission switch (Ile114$^{3.40}$, Pro196$^{5.50}$, Leu197$^{5.51}$, Phe281$^{6.44}$, Trp285$^{6.48}$); and Met203$^{5.57}$ sits above the tyrosine of the DRY motif (Asp130$^{3.49}$, Arg131$^{3.50}$, Tyr132$^{3.51}$). Using the inactive α_{1A}-AR variant, α_{1A}-AR-A4, and by reverse mutation to an active receptor (α_{1A}-AR-A4-active) we show that for Met115$^{3.41}$ and Met203$^{5.57}$ the chemical shifts and line-widths of the $^{13}C^{\varepsilon}H_3$ groups are dependent on ligand efficacy (from strong inverse agonist to full agonist), suggesting that α_{1A}-AR activation proceeds primarily through a conformational selection mechanism.

Results

$^{13}C^{\varepsilon}H_3$ methionine labelling and NMR signal assignment

α_{1A}-AR-A4 is a thermostabilised variant of the human α_{1A}-AR that contains 15 amino acid substitutions over wild type (WT) human α_{1A}-AR (Supplementary Figure 1). Excluding Met1, α_{1A}-AR-A4 possesses six methionine residues, five of which are naturally occurring (Met115$^{3.41}$, Met145$^{4.44}$, Met203$^{5.57}$, Met248^{ICL3}, Met292$^{6.55}$) and one, Met80$^{2.58}$, is a thermostabilising mutation previously selected for (Yong et al., 2018) (Supplementary Figure 1). Homology models of α_{1A}-AR (Figure 1) built on in inactive- and active-states of X-ray structures of β_2-AR show that three of these methionines were particularly interesting as conformational probes as they are located either within the adrenaline binding site (Met292$^{6.55}$), immediately adjacent to the highly conserved Ile114$^{3.40}$ of the transmission switch (Met115$^{3.41}$), or sitting above Tyr125$^{3.51}$ of the DRY motif within the G protein binding site (Met203$^{5.57}$). These homology models of α_{1A}-AR suggest that each of these regions undergo significant local rearrangements between inactive to active conformations (Figure 1).

α_{1A}-AR-A4 was expressed and labelled with $^{13}C^{\varepsilon}H_3$-methionine using an adapted *E. coli* methionine biosynthesis pathway inhibition protocol that we have previously used to

generate $^{13}C^{\varepsilon}H_3$-methionine-labeled neurotensin receptor 1 (NTS_1) samples labelled with 96% incorporation efficiency(Bumbak et al., 2019; Bumbak et al., 2018). Using this method α_{1A}-AR-A4 expressed well and could be purified, solubilized in n-dodecyl β-D-maltopyranoside (DDM), with a yield of (0.5-1 mg/L culture). 40-60 µM samples of $^{13}C^{\varepsilon}H_3$-methionine-labeled α_{1A}-AR-A4 were subsequently used to record 2D ^{1}H-^{13}C SOFAST-heteronuclear multiple quantum coherence (HMQC) spectra in the apo state, and in the bound states for prazosin (full inverse agonist), WB-4101 (partial inverse agonist), phentolamine (partial inverse agonist), silodosin (or KMD-3213, neutral antagonist), oxymetazoline (partial agonist) and adrenaline (full agonist) (Figure 2 and Supplementary Figure 2). Individual $^{13}C^{\varepsilon}H_3$-methionine resonances were assigned by expressing and analysing α_{1A}-AR-A4 M80L, α_{1A}-AR-A4 M115I, α_{1A}-AR-A4 M203L, α_{1A}-AR-A4 M248I and α_{1A}-AR-A4 M292I mutants in the same way. ^{1}H-^{13}C SOFAST-HMQC spectra enabled clear assignment of mutated methionines as the remaining five resonances in these spectra showed only small chemical shift differences in the presence of the mutation (Supplementary Figure 3). The $^{13}C^{\varepsilon}H_3$-methionine of the apo state of α_{1A}-AR-A4 showed clear single resonances for each methyl with no significant heterogeneity, in contrast to many previously studied GPCRs (Casiraghi et al., 2016; Kofuku et al., 2012; Nygaard et al., 2013; Okude et al., 2015; Solt et al., 2017; Xu et al., 2019), (Figure 2). $Met145^{4.44}$ and $Met248^{ICL3}$ exhibited intense signals with ^{1}H and ^{13}C chemical shifts of the methyl group indicative of solvent exposed, unrestrained methyl groups. $Met248^{ICL3}$, located within ICL3 (Figure 1a), showed strong signal intensity most likely due to the mobility of this loop and exposure to the bulk solvent. $Met145^{4.44}$ is at the C-terminal intracellular end of TM4, predicted to be exposed on the surface of the helix (Figure 1a) and thus also highly mobile. $Met80^{2.58}$ was not unambiguously assigned (Supplementary Figure 3a,f) as it either is significantly broadened and difficult to resolve in all receptor states or may overlap with $Met145^{4.44}$ and under some conditions with $Met292^{6.55}$ (Supplementary

Figure 3e). The remaining methionines, Met115$^{3.41}$, Met203$^{5.57}$ and Met292$^{6.55}$, were readily assigned (Supplementary Figure 3b,c,e,g,h,j) and exhibited resolved chemical shifts for the $^{13}C^{\varepsilon}H_3$ that were sensitive to the bound ligand (Figure 2b-d).

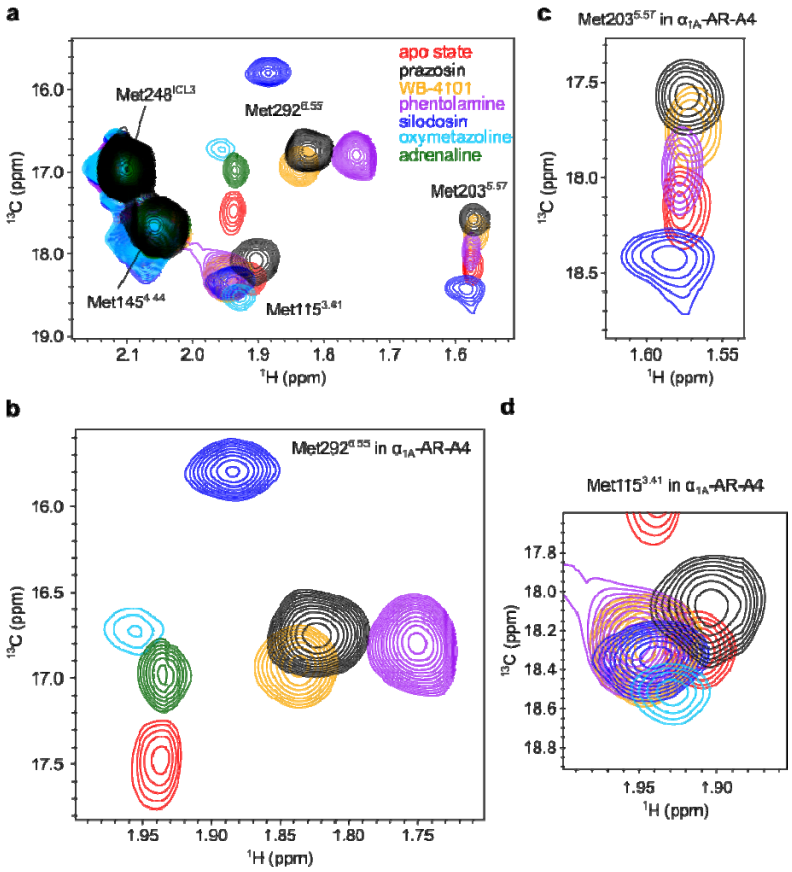

Figure 2. ^{1}H-^{13}C SOFAST-HMQC spectra of α_{1A}-AR-A4. (a) Overlay of 2D ^{1}H-^{13}C SOFAST-HMQC spectra for [$^{13}C^{\varepsilon}H_3$-Met] α_{1A}-AR-A4 collected in the apo state (red) and bound to prazosin (black, inverse agonist), WB-4101 (yellow, inverse agonist), phentolamine (purple, inverse agonist), silodosin (blue, neutral antagonist), oxymetazoline (cyan, partial agonist) and adrenaline (green, full agonist). (b) Close-up of the Met292$^{6.55}$ resonance. (c) Close-up of the Met203$^{5.57}$ resonance. (d) Close-up of the Met115$^{3.41}$ resonance. Spectra were acquired on ~50 μM α_{1A}-AR-A4 dissolved in 0.02-0.1% DDM micelle, pH 7.5 and 25 °C.

Based on homology models, Met292$^{6.55}$ projects into the orthosteric ligand binding pocket (Figure 1a) and mutational studies support a role for this residue in ligand binding (Hwa et al., 1995). Thus, the $^{13}C^{\varepsilon}H_3$ chemical shifts of Met292$^{6.55}$ likely reflect a direct interaction with chemical groups of each ligand. Interestingly, the resonance intensities of Met292$^{6.55}$ increased in the presence of antagonists and inverse agonists relative to the apo state (Figure 2b), indicating that binding of these ligands reduces conformational dynamics in the orthosteric binding site. Met115$^{3.41}$ and Met203$^{5.57}$ are distant from the orthosteric site, but both the chemical shifts and linewidths of their $^{13}C^{\varepsilon}H_3$ groups were sensitive to ligand binding (Figure 2c,d), likely reflecting receptor conformational changes in the transmission switch and G protein-binding site respectively (Figure 1c,d). The ^{1}H chemical shift of the methyl of Met203$^{5.57}$ was shifted upfield from typical small-peptide positions (2.1 ppm) to 1.58 ppm in agreement with our models, which predict ring-current induced effects from Tyr125$^{3.51}$ of the DRY motif (Supplementary Figure 4). Met203$^{5.57}$ therefore serves as a probe of conformational change within this region. Indeed, the resonances of the $^{13}C^{\varepsilon}H_3$ of Met203$^{5.57}$ exhibited a significant linear chemical shift change depending on which ligand was bound, demonstrating that allosteric coupling between the ligand binding site and the G protein-binding site is retained in the inactive α_{1A}-AR-A4 in solution. Such a linear chemical shift change is also expected for ligands modulating receptor state *via* conformational selection. We postulate that the Met203$^{5.57}$ signal reflects the average, equilibrium signal, between inactive and active states undergoing fast exchange. Inverse agonists preferentially bound to inactive states, shifting the Met203$^{5.57}$ equilibrium to an upfield position (inactive state) compared to apo state receptor, which can sample active-like states to a certain degree.

We were interested to see if an opposite trend could be observed for receptor agonists, which we hypothesised would shift the position of the Met203$^{5.57}$ resonance downfield. For α_{1A}-AR-A4 however, the binding of the full agonist adrenaline to α_{1A}-AR-A4 resulted in

complete line broadening of the Met115$^{3.41}$ and Met203$^{5.57}$ resonances despite the promotion of a distinct chemical shift for Met292$^{6.55}$ in the binding site. Binding of the partial agonist oxymetazoline resulted in substantial broadening of Met203$^{5.57}$ and Met292$^{6.55}$, but not Met115$^{3.41}$. The loss of these chemical shifts upon agonist binding was likely due to the significantly weaker agonist affinities at α_{1A}-AR-A4 compared to unmutated, WT α_{1A}-AR, as a result of the F312L stabilizing mutation (Yong et al., 2018). Thus, NMR experiments were repeated on α_{1A}-AR-A4 (L312F), for which agonist affinities were largely restored to that of WT α_{1A}-AR (Supplementary Figure 5 and Supplementary Table 1) (Yong et al., 2018).

Agonist induced chemical shifts of Met115$^{3.41}$ and Met203$^{5.57}$ resonances

Despite the reduced thermostability of α_{1A}-AR-A4 (L312F) (Yong et al., 2018), we were able to $^{13}C^{\varepsilon}H_3$-methionine-label and record ^{1}H-^{13}C SOFAST-HMQC spectra for this receptor in the apo state and bound to adrenaline (full agonist), phenylephrine (full agonist), A-61603 (full agonist), and oxymetazoline (partial agonist) in addition to the inverse agonists and neutral antagonists tested on α_{1A}-AR-A4 (Figure 3a). Overall the ^{1}H-^{13}C SOFAST-HMQC spectra of the apo, antagonist and inverse agonist bound states of α_{1A}-AR-A4 (L312F) were similar to those of α_{1A}-AR-A4. Again, single resonances for the $^{13}C^{\varepsilon}H_3$-methionine groups of α_{1A}-AR-A4 (L312F) were observed for all ligands. The chemical shifts of Met292$^{6.55}$ induced by each ligand in α_{1A}-AR-A4 (L312F) were slightly different to those of α_{1A}-AR-A4, most likely due to orthosteric binding site changes after the L312F reversion. Inverse agonist binding increased the intensity of the Met292$^{6.55}$ resonance in α_{1A}-AR-A4 (L312F), as was seen with α_{1A}-AR-A4; whereas the neutral antagonist silodosin significantly decreased the peak intensity and the partial agonist oxymetazoline and full agonist A-61603 highly broadened the resonance of Met292$^{6.55}$ in α_{1A}-AR-A4 (L312F) (Supplementary Figure 6).

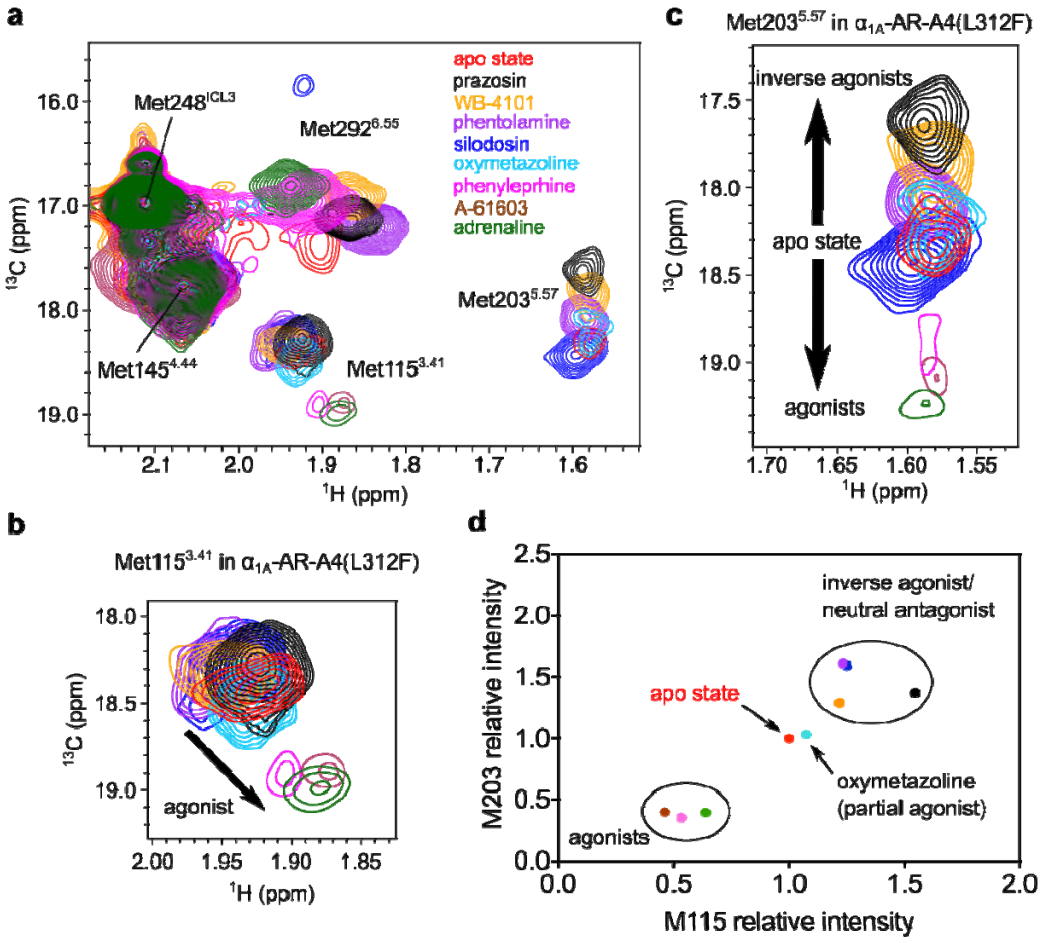

Figure 3. Ligand efficacy-dependent chemical shifts of Met115$^{3.41}$ and Met203$^{5.57}$ resonances. (a) Overlay of 2D ^{1}H-^{13}C SOFAST-HMQC spectra for [^{13}C$^{\varepsilon}$H$_3$-Met] α_{1A}-AR-A4 (L312F) in the apo state (red) and bound to ligands: prazosin (black, inverse agonist), WB-4101 (orange, inverse agonist), phentolamine (purple, inverse agonist), silodosin (blue, neutral antagonist), oxymetazoline (cyan, partial agonist), phenylephrine (magenta, full agonist), A-61603 (maroon, full agonist), adrenaline (green, full agonist). (b) Close-up of the Met115$^{3.41}$ resonance in α_{1A}-AR-A4 (L312F). (c) Close-up of the Met203$^{5.57}$ resonance in α_{1A}-AR-A4 (L312F). The spectra for adrenaline, A-61603 and phenylephrine are plotted at a level 1.8-times lower than the main figure. (d) Normalized peak intensities of Met115$^{3.41}$ and Met203$^{5.57}$ of α_{1A}-AR-A4 (L312F) show differences between agonists, antagonists and partial agonists. Ligands are coloured as listed above. Spectra were acquired on ~50 μM α_{1A}-AR-A4 (L312F) dissolved in 0.02-0.1% DDM micelle, pH 7.5 and 25 °C.

The recovered agonist affinity for α_{1A}-AR-A4 (L312F) allowed the measurement of ^{1}H-^{13}C SOFAST-HMQC spectra where we were confident of full receptor-agonist saturation. Binding of the full agonist adrenaline to α_{1A}-AR-A4 (L312F) produced a similar Met292$^{6.55}$ chemical shift to that seen with α_{1A}-AR-A4 (Figure 3a), and also weak peaks were now observed for Met115$^{3.41}$ and Met203$^{5.57}$ (Figure 3b,c), which were completely broadened in adrenaline-bound α_{1A}-AR-A4. Importantly, the binding of all agonists, adrenaline, phenylephrine and A-61603 to α_{1A}-AR-A4 (L312F) induced distinct chemical shift and line broadening changes to Met115$^{3.41}$ and Met203$^{5.57}$ compared to neutral antagonists and inverse agonists (Figure 3b,c). The agonist-induced Met115$^{3.41}$ resonances cluster together potentially indicative of an active transmission switch conformation (Figure 3b). Binding of the partial agonist oxymetazoline induced a chemical shift of Met115$^{3.41}$ falling between the inverse agonist and full agonist clusters, consistent with partial agonists promoting a weaker shift in the inactive-active transmission switch state equilibrium. The linear change in Met203$^{5.57}$ chemical shift position upon inverse agonist binding seen with α_{1A}-AR-A4 was retained in α_{1A}-AR-A4 (L312F), but as hypothesised, agonist binding promoted opposite, downfield resonance shifts in the ^{13}C dimension along the same vector (Figure 3c). This change in $^{13}C^{\varepsilon}H_3$-methionine chemical shift in the ^{13}C dimension reflects a change in the $\chi 3$ dihedral angle. The ^{13}C chemical shift dependence of this angle is about 19 ppm for trans and 16 ppm for ±gauche (Butterfoss et al., 2010). For the apo and antagonist states the chemical shift of 18.25 to 18.5 ppm suggests a trend toward trans, whereas in the full-inverse agonist state the resonance shifts up-field to 17.7 ppm, indicative of an averaging between gauche and trans. Consistent with our homology models (Supplementary Figure 4) for full agonist a further downfield shift between 19 to 19.25 ppm infers an increase in the trans conformer. Interestingly, the partial agonist oxymetazoline induced a small upfield $^{13}C^{\varepsilon}$ shift of Met203$^{5.57}$, similar to the inverse agonist phentolamine. The fact that full agonists induced

289 Met203$^{5.57}$ chemical shifts to move in the opposite direction to inverse agonists suggests an
290 equilibrium shift away from inactive to active conformational states of the DRY motif.
291 Furthermore, the resonance intensities of both Met115$^{3.41}$ and Met203$^{5.57}$ in α_{1A}-AR-A4
292 (L312F), relative to the ligand-insensitive Met145$^{4.44}$ resonance, were weakened upon agonist
293 binding compared to the intensity increases seen with antagonists and inverse agonists
294 (Figure 3d). The intensities of Met115$^{3.41}$ and Met203$^{5.57}$ upon binding of the partial agonist
295 oxymetazoline fell in between the antagonist- and agonist-induced intensities. The behaviour
296 of the $^{13}C^{\varepsilon}H_3$ of Met115$^{3.41}$ and Met203$^{5.57}$ is consistent with the current concept that agonists
297 increase conformational heterogeneity in GPCRs, where agonists increase microsecond
298 timescale transitions to active receptor states, to increase the probability of engaging and
299 activating effector proteins (Kofuku et al., 2012; Manglik et al., 2015; Nygaard et al., 2013;
300 Shimada et al., 2018; Solt et al., 2017; Ye et al., 2016).
301
302 **Chemical shift changes of Met203$^{5.57}$ correlate with ligand efficacy.**
303 In mammalian cells, α_{1A}-AR exhibits basal activity in the absence of bound ligands(Zhu et
304 al., 2000). Such basal activity is unaffected by the binding of neutral antagonists but is
305 reduced by the binding of inverse agonists to the receptor. In the case of α_{1A}-AR, by probing
306 the ability of various antagonists to reduce the signalling of a constitutively active receptor
307 mutant, the rank order of inverse agonist efficacies has been found to be: prazosin (strongest);
308 WB-4101; phentolamine (weakest); and silodosin being a neutral antagonist (Zhu et al.,
309 2000). To understand how the NMR signals of Met203$^{5.57}$ in α_{1A}-AR-A4 (L312F) relate to
310 receptor conformational equilibria, the changes to the chemical shifts for the $^{13}C^{\varepsilon}H_3$ of
311 Met203$^{5.57}$ were plotted against the previously published relative efficacy values for the
312 inverse agonists, revealing a strong linear correlation ($R^2 = 0.99$, Figure 4a). To test if this
313 correlation is retained when probing inverse agonism at the wild-type α_{1A}-AR, we determined

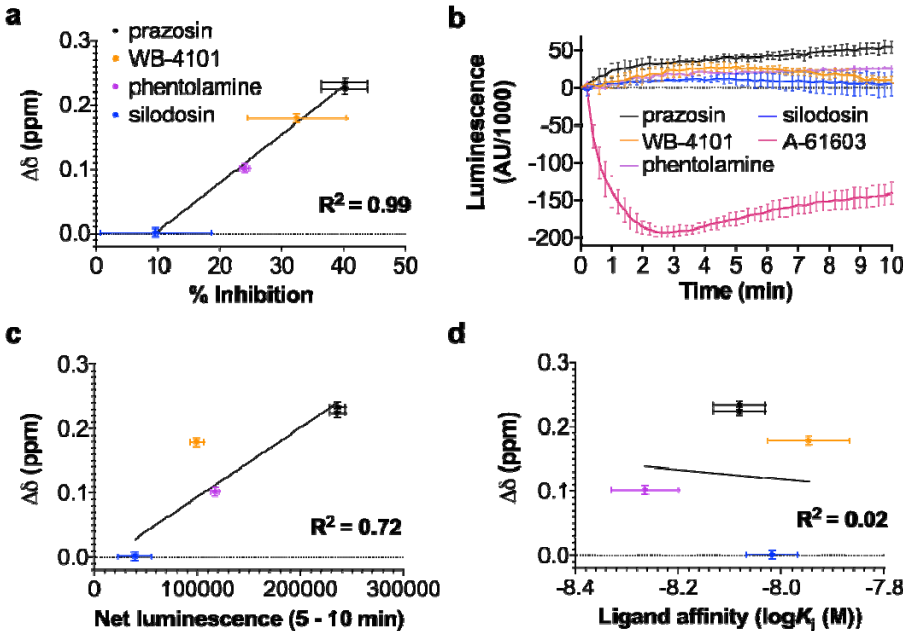

Figure 4. Correlation between the chemical shift positions of the $^{13}C^{\varepsilon}H_3$ in Met203$^{5.57}$ and inverse agonists efficacy. (a) Linear regression analysis of the average chemical shift differences (Δδ) for the $^{13}C^{\varepsilon}H_3$ of Met203$^{5.57}$ in α_{1A}-AR-A4 (L312F) when bound to prazosin (black circles), WB-4101 (orange circles), and phentolamine (purple circles) compared to silodosin (blue circles) and the published efficacy of each ligand in reducing the signaling of a constitutively active mutant of α_{1A}-AR (Zhu et al., 2000). Published data were extracted using WebPlotDigitizer (https://automeris.io/WebPlotDigitizer). Testing the resultant equation against the null hypothesis of a slope of zero resulted in a P value of < 0.0001 (b) NanoBit G protein activity assay demonstrating inverse agonism of prazosin, WB-4101, phentolamine and silodosin at WT α_{1A}-AR-expressing COS-7 cells. Each of these inverse agonist experiments were repeated in three independent biological replicate experiments, with the mean ± SEM of the resultant luminescence plotted for each timepoint. To demonstrate the response from an agonist, A-61603 treatment was performed in two independent biological replicate experiments. Each biological replicate comprised three technical replicates measured in parallel. The grey shaded region indicates where the area under each biological replicate curve was calculated for (c). (c) Linear regression analysis of the average chemical shift differences (Δδ) for the $^{13}C^{\varepsilon}H_3$ of Met203$^{5.57}$ in α_{1A}-AR-A4 (L312F) and the increase in luminescence seen in the NanoBit assay for each inverse agonist and neutral antagonist. Ligands are coloured as listed above

and the P value testing against a slope of 0 was 0.011 (d) Linear regression analysis of the average chemical shift differences (Δδ) for the $^{13}C^{\varepsilon}H_3$ of Met203$^{5.57}$ in α_{1A}-AR-A4 (L312F) and the affinities of each inverse agonist and neutral antagonist. Ligands are coloured as listed above and the P value testing against a slope of 0 was 0.89. In (a), (c) and (d) Δδ are plotted for two independent titrations of prazosin and silodosin, and single experiments for WB-4101 and phentolamine. Average chemical shift differences (Δδ) were normalised using the equation $\Delta\delta=[(\Delta\delta_{1H})^2+(\Delta\delta_{13C}/3.5)^2]^{0.5}$ and error were calculated by the formula $[\Delta\delta_{1H}*R_{1H}+\Delta\delta_{13C}*R_{13C}/(3.5)^2]/\Delta\delta$, where R_{1H} and R_{13C} are the digital resolutions in ppm in the ^{1}H and ^{13}C dimensions respectively (Kofuku et al., 2012).

the relative inverse agonist efficacies of these ligands using a NanoBiT split luciferase assay (Inoue et al., 2019). In this assay the 18 kDa Large BiT (LgBiT) fragment was fused to the N-terminus of $G\alpha_q$ and the 1.3 kDa Small BiT (SmBiT) was fused to the N-terminus of $G\gamma_2$. When co-expressed with $G\beta_1$, the formation of a $G\alpha_q$(LgBiT)-$G\beta_1$-$G\gamma_2$(SmBiT) heterotrimer results in bright luminescence. GPCR-induced stimulation of this G protein complex causes dissociation of the heterotrimer and thus reduction in luminescence output, whereas inhibition of basal GPCR activation would be predicted to increase luminescence output. COS-7 African green monkey kidney cells stably expressing wild-type (WT) α_{1A}-AR were transfected with $G\alpha_q$(LgBiT), $G\beta_1$ and $G\gamma_2$(SmBiT) encoding expression plasmids, incubated with luminescence substrate, and then treated with various α_{1A}-AR ligands while monitoring cellular luminescence. A-61603 induced α_{1A}-AR activation led to heterotrimer dissociation of the $G\alpha_q$(LgBiT)-$G\beta_1$-$G\gamma_2$(SmBiT) complex and thus a reduction in luminescence output (Figure 4b). Inverse agonists on-the-other-hand reduced basal activation of α_{1A}-AR, maintaining the $G\alpha_q$(LgBiT)-$G\beta_1$-$G\gamma_2$(SmBiT) complex leading to increase luminescence output from the cells (Figure 4b). The specificity of these responses was probed by conducting the same experiments on COS-7 cells not expressing α_{1A}-AR (Supplementary Figure 7a-c). The observed changes in luminescence after α_1-AR ligand treatments were

specific to α_{1A}-AR expressing cells except for WB-4101, which induced a short (5 min) increase in luminescence in the control cells (Supplementary Figure 7a). To exclude this non-specific effect the net luminescence change for each sample group was calculated as the area under the luminescence curves between 5 and 10 min after ligand addition. A strong linear correlation was found between the chemical shift changes for the $^{13}C^{\varepsilon}H_3$ of Met203$^{5.57}$ in α_{1A}-AR-A4 (L312F) and the net luminescence increase generated by each inverse agonist over the five-minute period in the WT α_{1A}-AR-expressing cells (R^2 = 0.72, Figure 4c). Importantly, the Met203$^{5.57}$ chemical shift positions of α_{1A}-AR-A4 (L312F) did not correlate with the affinity of these antagonists for α_{1A}-AR (Figure 4d), demonstrating that the differences in chemical shift were not due to varying receptor occupancy. Furthermore, no correlation was seen between the $^{13}C^{\varepsilon}H_3$ Met203$^{5.57}$ chemical shift changes of α_{1A}-AR-A4 (L312F) and the net luminescence changes in COS-7 cells not expressing WT α_{1A}-AR (Supplementary Figure 7b). Critically, the correlation between chemical shift changes of $^{13}C^{\varepsilon}H_3$ Met203$^{5.57}$ in α_{1A}-AR-A4 (L312F) and WT α_{1A}-AR-specific luminescence increases in the NanoBiT assay remained when the analysis window was extended to include the full 10 minutes after ligand addition (Supplementary Figure 7d).

Improving signalling competency in α_{1A}-AR-A4

When expressed in COS-7 cells, α_{1A}-AR-A4 is incapable of stimulating cellular increases in IP_1 in response to adrenaline binding, or activation of a cyclic adenosine monophosphate (cAMP) response element (CRE) reporter gene after treatment with another α_1-AR agonist, phenylephrine (Yong et al., 2018). To ensure biological relevance of our NMR studies we thus sought α_{1A}-AR-A4 back-mutants that were able to stimulate canonical signalling pathways in mammalian cells upon agonist treatment. Seven thermostabilising mutations within the TMD of α_{1A}-AR-A4 were back-mutated (Y67N, M80L, A127G, F151W, K322N,

L327P and Y329S) as single changes or in combinations, and screened for phenylephrine and oxymetazoline induced signalling with an IP_1 assay in transfected COS-7 cells (Supplementary Figure 8a). While the back-mutant, α_{1A}-AR-A4 (Y67N, M80L, K322N, L327P, Y329S) was able to facilitate significant oxymetazoline-induced cellular accumulation of IP_1 compared to α_{1A}-AR-A4 and WT α_{1A}-AR (Supplementary Figure 8a) it expressed poorly in bacteria. The back-mutant α_{1A}-AR-A4 (Y67N, K322N), termed α_{1A}-AR-A4-active, however was able to stimulate IP_1 accumulation in response to both phenylephrine and oxymetazoline treatment (Supplementary Figure 8a) and it expressed well in bacteria. Importantly, α_{1A}-AR-A4 contains the N322K-stabilising mutation in the NPxxY switch(Trzaskowski et al., 2012), which is hypothesised to form a stabilizing salt bridge with Asp72$^{2.50}$ to lock the NPxxY switch in an inactive and stable state. We thus expected that reversion of this mutation (K322N) would restore the function of the NPxxY switch and the signalling activity of α_{1A}-AR-A4. Interestingly, the Y67N mutation was required on top of K322N to restore signalling activity in α_{1A}-AR-A4-active. N67$^{2.45}$ is distant from the NPxxY switch and its importance is not clear.

Using an intracellular calcium mobilisation assay, α_{1A}-AR-A4-active was able to be activated by the full agonists adrenaline and A-61603, as well as the partial agonists oxymetazoline and PF-3774076 (Supplementary Figure 8b-e). The affinity of QAPB for α_{1A}-AR-A4-active was retained upon purification of the receptor in DDM (Supplementary Figure 9a). Competition binding assays revealed however, that the affinities of agonists for α_{1A}-AR-A4-active (Supplementary Figure 9b and Supplementary Table 1) were weaker than WT α_{1A}-AR due to the F312L stabilizing mutation, but stronger than at α_{1A}-AR-A4 (Yong et al., 2018). When purified in DDM α_{1A}-AR-A4-active was significantly less stable than α_{1A}-AR-A4 (Supplementary Figure 9c) and thus back-mutation of F312L to recover agonist potency was not pursued as it was deemed unlikely that the resultant receptor would be stable enough

for NMR experiments.

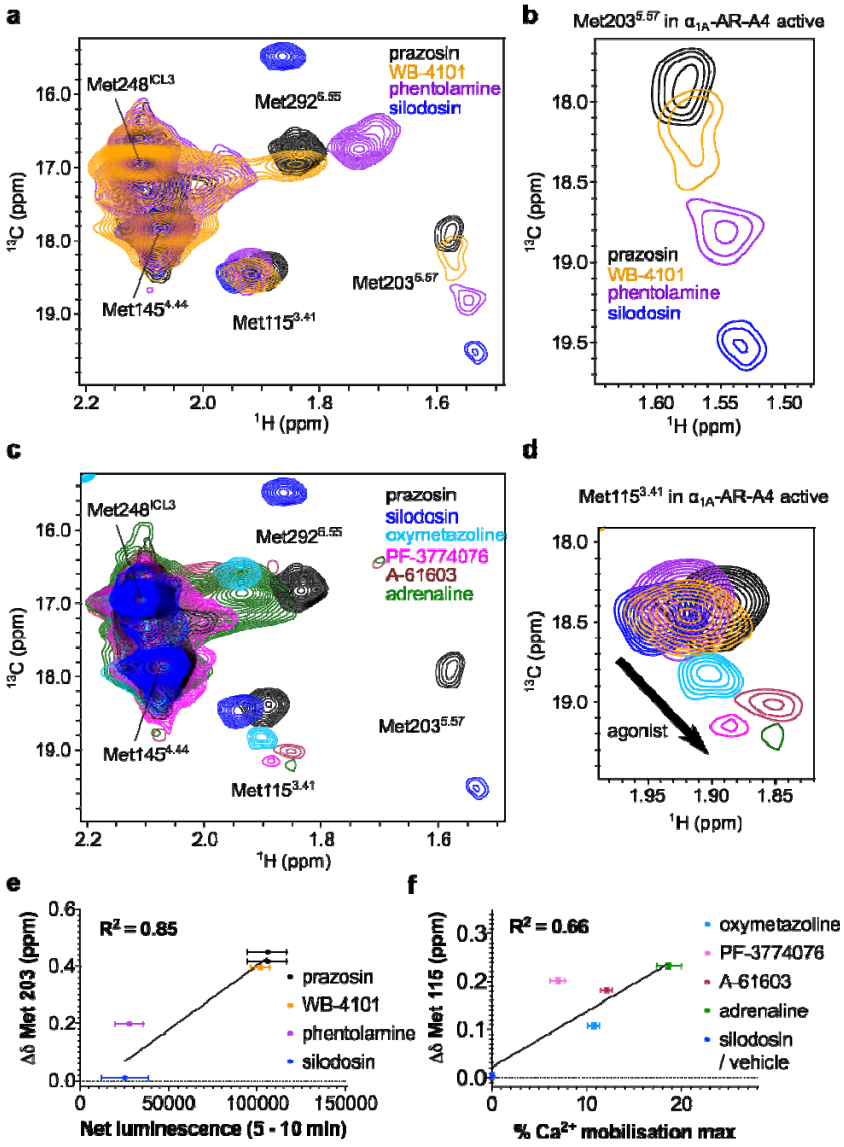

Figure 5. ^{1}H-^{13}C SOFAST-HMQC spectra of α_{1A}-AR-A4-active. (a) Overlay of 2D ^{1}H-^{13}C SOFAST-HMQC spectra of [$^{13}C^{\varepsilon}H_3$-Met] α_{1A}-AR-A4-active bound to prazosin (black, inverse agonist), WB-4101 (yellow, inverse agonist), phentolamine (purple, inverse agonist) and silodosin (blue, neutral antagonist). (b) Close-up of the Met203$^{5.57}$ resonance. (c) Overlay of 2D ^{1}H-^{13}C SOFAST-HMQC spectra of [$^{13}C^{\varepsilon}H_3$-Met] α_{1A}-AR-A4-active bound to prazosin (black, inverse agonist), silodosin (blue, neutral antagonist), oxymetazoline (cyan, partial agonist), PF-3774076 (magenta, partial agonist), A-61603 (maroon, full agonist), and adrenaline (green, full agonist). (d)

418 Close-up of the Met115$^{3.41}$ resonance. (e) Linear regression analysis of the average chemical shift
419 differences (Δδ) for the $^{13}C^{\varepsilon}H_3$ of Met203$^{5.57}$ in α_{1A}-AR-A4-active when bound to prazosin (black
420 circles), WB-4101 (orange circles), and phentolamine (purple circles) compared to silodosin (blue
421 circles) and the increase in luminescence seen in the NanoBit assay with α_{1A}-AR-A4-active
422 expressing COS-7 cells treated with the same antagonist (from Supplementary Figure 11a). Testing
423 the resultant equation against the null hypothesis of a slope of zero resulted in a P value of 0.0041 (f)
424 Linear regression analysis of the average chemical shift differences (Δδ) for the $^{13}C^{\varepsilon}H_3$ of Met115$^{3.41}$
425 in α_{1A}-AR-A4-active when bound to oxymetazoline (cyan circles), PF-3774076 (pink circles), A-
426 61603 (dark red circles), adrenaline (green circles) and silodosin (blue circles) and the efficacy of
427 each agonist in triggering Ca^{2+} mobilization in α_{1A}-AR-A4-active expressing COS-7 cells (from
428 Supplementary Figure 8b-e). Testing the resultant equation against the null hypothesis of a slope of
429 zero resulted in a P value of 0.0154 In (e) and (f) Δδ are plotted for two independent titrations of
430 prazosin, silodosin and oxymetazoline, and single experiments for other ligands. In (a-d) spectra were
431 acquired on ~50 μM α_{1A}-AR-A4-active dissolved in 0.02-0.1% DDM micelle, pH 7.5 and 25 °C.
432 Average chemical shift differences (Δδ) were normalised using the equation
433 $\Delta\delta=[(\Delta\delta_{1H})^2+(\Delta\delta_{13C}/3.5)^2]^{0.5}$ and errors were calculated by the formula
434 $[\Delta\delta_{1H}*R_{1H}+\Delta\delta_{13C}*R_{13C}/(3.5)^2]/\Delta\delta$, where R_{1H} and R_{13C} are the digital resolutions in ppm in the ^1H and
435 ^{13}C dimensions respectively (Kofuku et al., 2012).
436
437 α_{1A}-AR-A4-active was labelled with $^{13}C^{\varepsilon}H_3$-methionine and 2D ^1H-^{13}C SOFAST-
438 HMQC spectra acquired as above (Figure 5a,c). Overall the ligand-perturbed chemical shifts
439 of the $^{13}C^{\varepsilon}H_3$-methionine resonances in α_{1A}-AR-A4-active were similar to those in α_{1A}-AR-
440 A4 and α_{1A}-AR-A4 (L312F), except for several key differences with the Met115$^{3.41}$ and
441 Met203$^{5.57}$ resonances. We acquired spectra of four independent preparations of apo α_{1A}-AR-
442 A4-active (four biological replicates) and found that in the absence of bound ligand the data
443 were not easily reproduced (Supplementary Figure 10a). The well resolved Met203$^{5.57}$ varied

444 between an intense peak, two peaks of similar intensity, or a peak of weak intensity.
445 Met115$^{3.41}$ persisted as a split peak, although the two components varied in intensity.
446 Importantly, in the presence of the most potent inverse agonist, prazosin, the resonances of
447 Met115$^{3.41}$ and Met203$^{5.57}$ were single peaks, and regardless of sample preparation, exhibited
448 the same chemical shifts. The $^{13}C^{\varepsilon}H_3$ Met115$^{3.41}$ resonance, as perturbed by prazosin, aligned
449 approximately with the upfield component of the resonance for apo α_{1A}-AR-A4-active
450 (Supplementary Figure 10b). In contrast, upon titration with the neutral antagonist, silodosin,
451 the peaks of Met115$^{3.41}$ also collapsed to a single resonance with identical chemical shifts,
452 but now aligned best with the downfield component of apo α_{1A}-AR-A4-active
453 (Supplementary Figure 10b). For the two partial inverse agonists, WB-4101 and
454 phentolamine, the $^{13}C^{\varepsilon}H_3$ resonance of Met115$^{3.41}$ was a single resonance, positioned midway
455 between the 'prazosin' (upfield) and 'silodosin' (downfield) peaks (Figure 5d). These trends
456 for ligand-efficacy were present in α_{1A}-AR-A4 and α_{1A}-AR-A4 (L312F), but were not as
457 distinct as now observed for α_{1A}-AR-A4-active, and notably the apo states for α_{1A}-AR-A4
458 and α_{1A}-AR-A4 (L312F) did not show two discrete peaks for Met115$^{3.41}$. Such apo state
459 sample-to-sample heterogeneity may suggest the presence of misfolded contaminants, but
460 upon the addition of prazosin or silodosin each of these samples gave identical spectra
461 (Supplementary Figure 10a), supporting the binding competency of the α_{1A}-AR-A4-active
462 samples. The diversity of apo state spectra likely reflects diversity of conformational states of
463 similar free energy. The addition of agonist again resulted in , a single resonance for $^{13}C^{\varepsilon}H_3$
464 Met115$^{3.41}$ that shifts upfield in ^{1}H and downfield in ^{13}C (Figure 5d). The trend in shifts of
465 these resonances, however, suggests they follow in a linear manner evolving from the
466 downfield (basal) signal of the apo state and reflects the selection of the active-like state.

467 A major difference between the spectra of α_{1A}-AR-A4 and α_{1A}-AR-A4-active,
468 however, was significantly increased line broadening of the Met203$^{5.57}$ signal of α_{1A}-AR-A4-

active in the apo state (Supplementary Figure 10a) and when bound to antagonists (Figure 5b). This broadening suggests that the DRY motif near the G protein-binding site of α_{1A}-AR-A4-active is more dynamic compared to α_{1A}-AR-A4, consistent with a receptor that more readily transitions between inactive and active-receptor states. Importantly, similar to α_{1A}-AR-A4 and α_{1A}-AR-A4 (L312F) variants, the $^{13}C^{\varepsilon}H_3$ of Met203$^{5.57}$ shows an efficacy-dependent linear $^{13}C^{\varepsilon}H_3$ chemical shift change in the presence of inverse agonist and neutral antagonist, trending to an upfield ^{13}C position ($\chi3$ of ±gauche) for the more potent inverse agonist (Figure 5a,b). Unexpectedly, the addition of silodosin (neutral antagonist) resulted in a significant ^{13}C downfield shift to near 19.5 ppm consistent with a trans $\chi3$ angle for Met203$^{5.57}$. Furthermore, similar to α_{1A}-AR-A4, the Met203$^{5.57}$ $^{13}C^{\varepsilon}H_3$ resonance of α_{1A}-AR-A4-active was near completely broadened in the presence of agonists.

NanoBiT G protein activity assays were performed on COS-7 cells expressing α_{1A}-AR-A4-active to determine relative inverse agonist efficacies. The inverse agonists reduced basal Gq activity in α_{1A}-AR-A4-active in a similar way to WT α_{1A}-AR expressing cells (Figure 4a and Supplementary Figure 11a). The net luminescence change induced by each inverse agonist at α_{1A}-AR-A4-active expressing cells correlated well, in a linear fashion, with the $^{13}C^{\varepsilon}H_3$ chemical shift changes of Met203$^{5.57}$ that each ligand induced at purified α_{1A}-AR-A4-active, when analysed over two separate time periods (Figure 5e and Supplementary Figure 11b). Interestingly, the agonist-induced chemical shift changes of $^{13}C^{\varepsilon}H_3$ Met115$^{3.41}$ showed a linear correlation with the efficacy of each agonist in Ca^{2+} mobilization assays on α_{1A}-AR-A4-active expressing COS-7 cells (Figure 5f) although the partial agonist PF-3774076 was a notable outlier. Overall these cell-based assays with the ligand efficacy-correlated chemical shift changes of Met115$^{3.41}$ and Met203$^{5.57}$ clearly demonstrate that a conformational selection mechanism underlies receptor function in cells.

494

Discussion

Recent spectroscopic studies have demonstrated that different classes of GPCR ligands distinctly alter the population of receptor states within the GPCR conformational equilibrium(Shimada et al., 2018). GPCR conformational changes are driven by defined structural changes in the microswitches (Ahuja and Smith, 2009; Deupi and Standfuss, 2011; Latorraca et al., 2017; Trzaskowski et al., 2012) (Figure 1) and, thus, how particular ligands affect the GPCR microswitch states likely underlies their pharmacological output as inverse, partial, full or biased agonists. Observing these effects, however, remains challenging. α_{1A}-AR was one of the first GPCRs to be cloned and pharmacologically characterised (Cotecchia et al., 1988) and is clinically targeted with agonists as nasal decongestants and antagonists for hypertension and BPH. Despite the importance of this receptor there are currently no three-dimensional structures of α_{1A}-AR, reflecting the inherent instability of this protein. Here, we demonstrate that prototypical ligands modulate the conformational equilibrium, as measured at the microswitches, of α_{1A}-AR in defined and predictable ways by $^{13}C^{\varepsilon}H_3$-methionine labelling α_{1A}-AR variants and monitoring the ^{1}H and ^{13}C chemical shifts of these methyl resonances in the presence of ligands of different efficacy,.

It is well accepted that the NMR signals of methionine methyl groups are sensitive to the local environment and the conformation of the methionine side chain (Kofuku et al., 2012; Nygaard et al., 2013). Many of the conclusions made in this study rely on Met115$^{3.41}$, a probe for the conformation of the transmission switch, and Met203$^{5.57}$ as a probe of the DRY motif that signifies intracellular TMD rearrangements for G-protein binding. In our model of α_{1A}-AR, Met203$^{5.57}$ sits over Tyr125$^{3.51}$ of the DRY motif but is distant from Arg124$^{3.50}$ which is expected to undergo significant rotameric changes within this motif (Carpenter and Tate, 2017) (Figure 1d). Met115$^{3.41}$ is sequential to the Ile114$^{3.40}$ in TM3 but it points away and is distant to transmission switch residue Phe281$^{6.44}$ located on TM6 that is expected to undergo

significant rotameric changes (Figure 1c). While in the thermostabilized inactive α_{1A}-AR-A4 mutant the residues of the transmission switch and DRY motif are retained, the asparagine of a third microswitch, the NPxxY motif, is mutated to lysine, which likely forms a salt bridge with Asp72$^{2.50}$ to lock this switch in an inactive state. The transmission switch and NPxxY motif are proximal to each other and therefore Met115$^{3.41}$, while distant to NPxxY, is likely to be sensitive to conformational changes involving both switches. In the reported active-state GPCR structures, three conserved residues (Arg$^{3.50}$ of the DRY motif, Tyr$^{7.53}$ of the NPxxY motif and Tyr$^{5.58}$) adopt near identical positions and connect these microswitches through water-mediated hydrogen bonds(Carpenter and Tate, 2017; Manglik and Kruse, 2017). Furthermore, in our model of active α_{1A}-AR which is based on structures of β_2-AR, Arg124$^{3.50}$ of the DRY motif is in contact with Tyr326$^{7.53}$ of the NPxxY motif (Figure 1d).

In our NMR experiments for all ligands the $^{13}C^{\varepsilon}H_3$ group of both Met115$^{3.41}$ and Met203$^{5.57}$ show significant directional chemical shift and line-width changes that are correlated with ligand efficacy, not affinity. As a distinct peak is observed for the addition of each ligand the chemical shift likely reflects an average population exchanging on a fast to intermediate timescale. The chemical shift differences, however, reflect a shift in the equilibrium, and specifically for the $^{13}C^{\varepsilon}H_3$ of Met203$^{5.57}$, from a $\chi 3$ of a gauche-trans average (inverse agonist) towards a trans (agonist) average (Figure 6a). An NMR study using ^{15}N-labelled, thermostabilised β_1AR observed substantial ligand efficacy-correlated backbone chemical shift changes for V226$^{5.57}$, which is in the same position as Met203$^{5.57}$ in α_{1A}-AR (Isogai et al., 2016). The authors speculated that these changes were caused by TM5 bending towards the active receptor state (Isogai et al., 2016), an idea that may also apply to α_{1A}-AR and other GPCRs. Here, the linear chemical shift changes of Met203$^{5.57}$, and to a lesser degree Met115$^{3.41}$, in response to ligands of different efficacy is strong evidence that agonists activate α_{1A}-AR via a conformational selection mechanism. The line broadening of

545 Met115$^{3.41}$ and Met203$^{5.57}$ upon agonist binding supports an efficacy-driven shift in dynamics,
546 and thereby the equilibrium of conformational states, communicated allosterically by the
547 microswitches and sensed by these methionine residues (Figure 6).
548

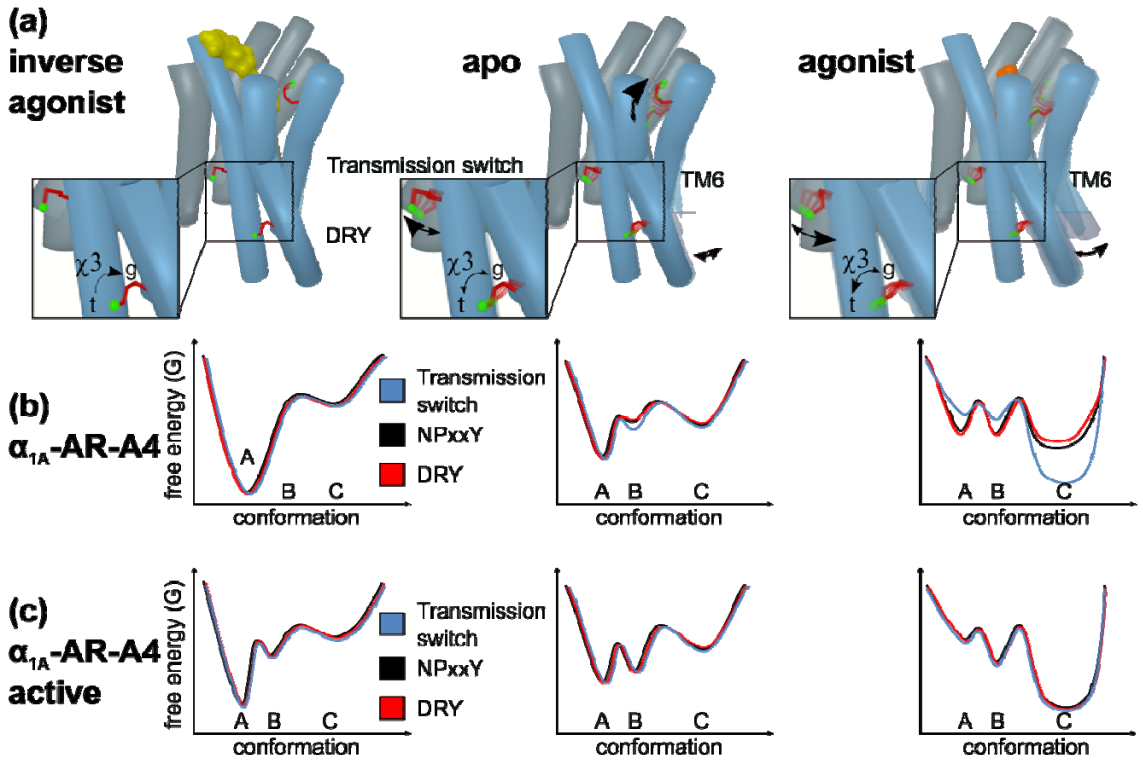

549

550 **Figure 6. How ligands modulate the conformational landscape of the α_{1A}-AR microswitches.** (a)
551 Cartoon representations of α_{1A}-AR in the inverse agonist-bound, apo, and agonist-bound states. The
552 three probe methionines, Met292$^{6.55}$ (binding site), Met115$^{3.41}$ (transmission switch) and Met203$^{5.57}$
553 (DRY microswitch) are highlighted with red sticks and the labeled methyl group in green. The arrows
554 labeled χ3 illustrate the ligand induced changes to the equilibrium between the trans (t) and gauche (g)
555 χ3 dihedral angle of Met203$^{5.57}$. Other arrows indicate how different ligands alter the conformation
556 equilibria of Met292$^{6.55}$, Met115$^{3.41}$ and TM6. Hypothetical free energy landscape diagrams of the
557 three microswitches in (b) the inactive α_{1A}-AR-A4 receptor compared to (c) α_{1A}-AR-A4-active. (A)
558 indicates the proposed inactive states, (B) represents basal states, and (C) represents active states of
559 the microswitches.

For our signalling incompetent receptors, α_{1A}-AR-A4 and α_{1A}-AR-A4 (L312F), the NPxxY microswitch has been mutated (N322K) in a way that would bias the NPxxY switch towards inactive states (K322 - D72 salt bridge). A consequence of this mutation is that for α_{1A}-AR-A4 (L312F) the DRY motif probe, Met203$^{5.57}$, gives relatively intense chemical shifts in the apo and antagonist-t-bound states (conformational equilibrium biased towards inactive states) (Figure 6b). On restoration of the NPxxY microswitch in α_{1A}-AR-A4-active however, the Met203$^{5.57}$ chemical shifts broaden and shift towards the agonist bound position (as defined for α_{1A}-AR-A4 (L312F)), even with neutral antagonist bound. Therefore, restoring the NPxxY microswitch enables the DRY motif of α_{1A}-AR-A4-active to more readily sample active-like states. The full trans (19.5 ppm in ^{13}C) populated by silodosin indicates that we may observe the full-active state, although previous studies showed that the full-active state is only populated in the presence of both agonist and nanobody (Manglik et al., 2015; Nygaard et al., 2013; Solt et al., 2017; Sounier et al., 2015; Xu et al., 2019). Our two methionine probes, Met115$^{3.41}$ and Met203$^{5.57}$, retain similar ligand-induced behaviour in α_{1A}-AR-A4-active compared to α_{1A}-AR-A4 and α_{1A}-AR-A4 (L312F), where the latter are both essentially inactive. The chemical shift and line-broadening trends of Met115$^{3.41}$ and Met203$^{5.57}$ suggest that the transmission switch and DRY motif, in the presence of an inactive NPxxY motif, can independently adopt conformations representative of active and inactive states. To fully adopt the conformational signatures of an active receptor, a functional NPxxY motif is required (in α_{1A}-AR-A4-active) thus increasing the dynamics of the transmission switch and DRY motif, suggesting that the interdependence of the three microswitches is a consequence of their dynamic nature, and that this is required for full receptor function.

While the striking linear chemical shift dependence for the $^{13}C^{\varepsilon}H_3$ of Met203$^{5.57}$ on ligand efficacy is consistent with a smooth change in equilibria from inactive to active, linear trends for $^{13}C^{\varepsilon}H_3$ of Met115$^{3.41}$ were less clear. In the inactive variants α_{1A}-AR-A4 and α_{1A}-

AR-A4 (L312F) the resonance for apo, inverse agonist and neutral antagonist shows little variation, but clear chemical shift changes and broadening are observed for agonists. The most distinct changes for the $^{13}C^{\varepsilon}H_3$ of Met115$^{3.41}$ were for α_{1A}-AR-A4-active, where in the apo-state two peaks were consistently observed, suggesting slow exchange (> millisecond) between two distinct states, to which we attribute to restoring the NPxxY microswitch. On the basis of chemical shift, we propose that the upfield peak of apo α_{1A}-AR-A4-active represents fully inactive receptor (state A in Figure 6), expected for full inverse agonists, and the downfield peak with a basal state receptor that is stabilized by the neutral antagonist (state B in Figure 6). This downfield 'basal' peak shows approximate linear efficacy-dependent chemical shift changes with agonist titrations. Therefore, the $^{13}C^{\varepsilon}H_3$ of Met115$^{3.41}$ reflects three states, (inverse agonist) inactive, an intermediate (basal) and active states (state(s) C in Figure 6), where the latter progressively shift from partial to full agonist states. Interestingly, in a $^{13}C^{\varepsilon}H_3$-methionine labelled study on the M2R, Met112$^{3.41}$, which is equivalent to Met115$^{3.41}$ in α_{1A}-AR, did not display efficacy-dependent chemical shift changes. In the presence of ligands, however, M2R Met112$^{3.41}$ was resolved as two separate resonances, consistent with a slow exchanging microswitch(Xu et al., 2019) and may highlight some differences between how different rhodopsin family GPCRs function.

In this NMR study, by starting with a signalling incompetent variant of α_{1A}-AR and subsequently restoring signalling activity through back mutations, we were able to study the functional dynamics of the key GPCR microswitches and how different ligands modulate this. Our NMR data for the transmission and DRY microswitches revealed ligand efficacy-dependent changes to the microswitch conformational equilibria, supporting a conformational selection mechanism for α_{1A}-AR modulation. This and the agonist-driven line broadening for both microswitches suggest similar mechanistic actions on the different microswitches, supporting ligand-driven allosteric communication between the microswitches. MD

simulations (Dror et al., 2011) of β_2-AR suggest that these microswitches behaved independently of each other, with only loose allosteric coupling. While this may be true over the relatively short timescales of MD, we believe that over the course of an NMR experiment such loose allosteric coupling culminates in significant coupled shifts to the microswitch conformations and that this is likely how ligands modulate GPCR signalling in cells.

Data Availability

All data that support the conclusions are included in the published paper and its supplementary information, or are available from the authors on request.

Acknowledgements

We thank Dr Fabian Bumbak (The Florey Institute of Neuroscience and Mental Health) for assistance with optimising the expression and purification of receptor samples; Prof. Dmitry Veprintsev (University of Nottingham) and Dr Franziska Heydenreich (Stanford University) for suggesting back mutations for the generation of α_{1A}-AR-A4-active; Prof. Asuka Inoue (Tohoku University) for supplying plasmids for the G protein activity assays; Sharon Layfield (The Florey Institute of Neuroscience and Mental Health) and Dr Ashish Sethi (The University of Melbourne) for assistance with cell-based assays and NMR data analysis respectively; Dr David Chalmers (Monash University) and the Monash University Medicinal Chemistry Computational Chemistry Facility for the assistance with computational modelling; The Bio21 NMR facility for access to spectrometers. This work was supported by NHMRC project grants 1081801 (D.J.S), 1081844 (P.R.G, D.J.S, R.A.D.B) and 1141034 (D.J.S, P.R.G, R.A.D.B). D.J.S. is an NHMRC Boosting Dementia Research Leadership Fellow.

636 **Author contributions**

637 FJW performed cloning, mutagenesis, protein expression and purification, thermostability
638 assays, acquisition and analysis of NMR data; LMW competition binding assays and
639 saturation binding assays; AAR intracellular Ca^{2+} mobilization assays; AG, MK, and RADB
640 NanoBiT G protein activity assays; TV computational modelling; ARW IP_1 assays. DJS,
641 MDWG and PRG conceived the experiments and with FJW analysed, prepared figures and
642 wrote the manuscript. All authors contributed to the editing of the manuscript.

643

644 **Competing financial interests**

645 The authors declare no competing financial interests.

646

647 **Methods**

648 **α_{1A}-AR constructs**

649 The α_{1A}-AR-A4 variant is a thermostabilised human α_{1A}-AR, containing 15 stabilising
650 mutations (Yong et al., 2018). $Met80^{2.58}$ in the spectra was introduced through the
651 stabilisation process in lieu of the naturally occurring amino acid leucine. As compared to
652 wild type, the carboxyl termini of the α_{1A}-AR-A4 variant was modified by truncation at
653 Ser351 and addition of a deca-His tag to facilitate purification (Supplementary Figure 1). For
654 expression, the α_{1A}-AR variants sequences were sub-cloned into the pQE30 derived vector,
655 pDS15, with a maltose-binding protein (MBP) and a methionine-free monomeric ultra-stable
656 green fluorescent protein (-Met-muGFP) (Scott et al., 2018) attached respectively to the N-
657 and C-termini of the receptor via HRV 3C protease cleavage sites. For the purpose of
658 Kingfisher binding assays, α_{1A}-AR variants were sub-cloned into a similar vector, pDS11, in
659 which muGFP was replaced with mCherry since the excitation and emission wavelengths of
660 fluorescent QAPB were overlapping with those of GFP. The final sequence of α_{1A}-AR-A4

after purification (with residues left from HRV 3C cleavage) is: GPGSVFLSGNASDSSNSIQPPAPVNISKAILLGVILGGIILFGVLGNILVILSVACHRHLH SVTHYYVVVYLAVADLLLTSTVMPFSAIYEVLGYWAFGRVFCNIWAAVDVLCCTASI MGLCIISIDRYIAVSYPLRYPTIVTQRRALMALLCVFALSLVISIGPLFGWRQPAPVDE TICQINEEPGYVLFSALGSFYLPLAIILVMYCRVYVVAKRESRGLKSGLKTDKSDSEQ VTLRIHRKNAPAGGSGMASAKTKTHFSVRLLKFSREKKAAKTLGIVVGCFVLCWLPF FLVMPIGSFFPDFKPSETVFKIVLWLGYLNSCIKPIIYLCYSQEFKKAFQNVLRIQCLCR KQSASHHHHHHHHHHGTRSLRGGLEVLFQ

In the α_{1A}-AR-A4 (L312F) variant one stabilising mutation L312 was reversed to phenylalanine to improve the affinity of ligands compared to α_{1A}-AR-A4. α_{1A}-AR-A4-active (Y67N, K322N) is a signalling competent variant in which the two stabilizing mutations Y67 and K322 were reverted to the wild-type asparagines. α_{1A}-AR-A4 was used for NMR assignment, where each methionine was substituted to either leucine or isoleucine. All mutations were introduced through site-directed mutagenesis using PrimeSTAR DNA polymerase (TaKaRa).

α_{1A}-AR expression

All α_{1A}-AR variants were expressed in *E. coli* C43 (DE3) cells (Lucigen, Middleton, WI). For $^{13}C^{\varepsilon}H_3$-methionine labelled expressions, 5 mL LB pre-culture containing 100 mg/L ampicillin and 1% (w/v) glucose was inoculated with a single colony of C43 cells freshly transformed with the expression plasmid and incubated at 37 °C, 225 rpm for approx. 8 h. 2 mL of the LB day culture was centrifuged (1700 rcf, 22 °C, 5 min) and the pellet was used to inoculate 100 mL of a defined minimal medium (M1 medium) (Bumbak et al., 2018) as overnight pre-culture. 10 mL of the overnight pre-culture was used to inoculate 500 mL of M1 medium in 2 L flasks. The expression cultures were incubated at 37 °C, 225 rpm to reach OD_{600} of 0.6, at

686 which point 50 mg/L $^{13}C^{\varepsilon}H_3$-methionine (Cambridge Stable Isotopes) was added along with
687 100 mg/L of each lysine, threonine, phenylalanine, and 50 mg/L of each leucine, isoleucine
688 and valine. The flasks were transferred to 20 °C and left shaking for 15 min prior to inducing
689 protein expression with 250 µM isopropyl β-D-1-thiogalactopyranoside (IPTG). After
690 overnight expression (15-18 h, 20 °C, 225 rpm), the culture was harvested by centrifugation
691 (2600 rcf, 4 °C, 15 min). The final pellet was snap frozen in liquid nitrogen and stored at -80
692 °C. For unlabelled expression 5 mL of LB pre-culture was used to inoculate 500 mL 2YT
693 medium containing 100 mg/L ampicillin and 0.4% (w/v) glucose. At OD_{600} of 0.6 the culture
694 was chilled on ice for 2 min prior to inducing protein expression with 250 µM IPTG
695 overnight expression and harvesting were carried out as described above.
696
697 **α_{1A}-AR purification**
698 The frozen cell pellet was thawed at room temperature for 30 min. 10 mL pellet was gently
699 resuspended in 40 mL ice-cold solubilisation buffer [25 mM HEPES, pH 7.5, 200 mM NaCl,
700 10% glycerol, 1% DDM (Anatrace), 0.12% CHS (cholesterol hemi succinate, Anatrace),
701 0.6% CHAPS (Sigma), 50 mg lysozyme, 5 mg Dnase, one tablet of EDTA free complete
702 protease inhibitor cocktail (Roche), 0.2-0.4 mM PMSF (phenylmethylsulfonyl fluoride)] and
703 incubated on a turning wheel for 30 min at 4 °C. The cell membranes were then disrupted by
704 sonication device (Diagenode Bioruptor Plus, high power, 10s on/20s off for 30 cycles)
705 followed by another 1 h incubation at 4 °C on the turning wheel. The cell debris was removed
706 by centrifugation (12,000 rcf, 4 °C, 40 min) and the supernatant was filtered using a 45 µm
707 Durapore syringe filter (Merck Millipore). The cleared cell lysate was incubated with 3 mL
708 Talon metal affinity resin pre-equilibrated with 45 mL equilibrium buffer (20 mM HEPES,
709 pH 7.5, 300 mM NaCl, 10% glycerol, 0.05% DDM). After 1.5 h incubation at 4 °C, the resin
710 retaining the receptor was washed three times with washing buffer 1 (20 mM HEPES, pH 7.5,

711 500 mM NaCl, 10% glycerol, 0.05% DDM) and then the full-length protein was eluted by 30
712 mL elution buffer (20 mM HEPES, pH 7.5, 300 mM NaCl, 10% glycerol, 0.05% DDM, 250
713 mM Imidazole). The eluate was concentrated down to 0.5-1 mL using a 100 kDa cut-off
714 centrifugal filter device (Amicon Ultra, Millipore). Imidazole was removed by using a PD10
715 desalting column (GE Healthcare). Cleavage of fusion proteins from the receptor was carried
716 out overnight at 4 °C by adding 100 mM Na_2SO_4, 1 mM TCEP and 300 pmol GST-tagged
717 HRV 3C protease (made in house).

718 The cleaved mixture was incubated for 1 h with 2 mL of pre-equilibrated Talon resin.
719 The resin was washed using 30 mL washing buffer 2 (20 mM HEPES, pH 7.5, 300 mM
720 NaCl, 10% glycerol, 0.05% DDM, 30 mM Imidazole) and the receptor was eluted by 20 mL
721 elution buffer. The eluate was concentrated down to 450 µL by 30 kDa cut-off centrifugal
722 filter device (Amicon Ultra, Millipore) and it was loaded onto a Superdex 200 10/300
723 increase column (GE healthcare) equilibrated with SEC buffer (50 mM sodium phosphate,
724 pH 7.5, 100 mM NaCl, 0.02% DDM). Size exclusion chromatography (SEC) was carried out
725 at a flow rate of 0.5 mL/min. The peak fractions containing receptor were pooled and
726 concentrated down to 100 µL using a 30 kDa cut-off centrifugal filter device (Amicon Ultra,
727 Millipore). The sample buffer was exchanged twice to NMR buffer (50 mM sodium
728 phosphate, pH 7.5, 100 mM NaCl, 99.9% D_2O). Yields were generally between 0.5-1 mg
729 receptor per litre of expression culture. Protein concentration was measured by BCA protein
730 assay (Pierce, ThermoFisher).

731

732 **NMR spectroscopy**

733 NMR samples were prepared to 130 µL at 40-60 µM receptor in a 3 mm Shigemi NMR tubes
734 (Shigemi Inc, Allison Park, PA). Ligands were added at saturating concentrations that were 2
735 mM adrenaline for α_{1A}-AR-A4 and α_{1A}-AR-A4 (active), 400 µM prazosin, and 1 mM of other

736 ligands to all mutants (supplementary Table 1). Adrenaline was supplemented with 1 mM of
737 the anti-oxidant ascorbic acid. Samples containing low affinity agonists (phenylephrine and
738 adrenaline) were recycled via competition with high affinity ligands, exchange was judged
739 via the chemical shift of the Met292$^{6.55}$ resonance. Experiments on α_{1A}-AR-A4 and α_{1A}-AR-
740 A4-L312F, apo and all ligands were performed at least twice on independent receptor
741 samples (biological replicates), except WB-4101 and phentolamine which were acquired
742 once. Experiments on apo α_{1A}-AR-A4-active and bound to prazosin, silodosin, and
743 oxymetazoline were performed at least twice on independent receptor samples, and for other
744 ligands were performed once.

745 All NMR spectra were collected at 25 °C on an 800-MHz Bruker Avance II
746 spectrometer equipped with a triple resonance cryoprobe. 2D ^{1}H-^{13}C SOFAST-HMQC
747 (Schanda et al., 2005) spectra were recorded by excitation with a 2.25 ms PC9 120 degree ^{1}H
748 pulse and refocusing with a 1 ms r-SNOB shaped 180 degree ^{1}H pulse. The spectral widths
749 were set to 12 ppm and 25 ppm for ^{1}H and ^{13}C dimensions respectively. For the spectra
750 recorded for α_{1A}-AR-A4 variant (Figure 2 and Supplementary Figure 3), 1024 x 128 complex
751 points were recorded with a 25% Poisson-gap sampling schedule and 2048 scans; an
752 acquisition time of 8.5 h. For the other spectra, 1024 x 200 complex points were recorded
753 with either traditional or 60% Poisson-gap sampling schedule and 368 scans resulting in
754 acquisition times of 10 h and 6 h respectively. Spectra were reconstructed with compressed
755 sensing using qMDD and processed using NMRpipe (Delaglio et al., 1995) where data were
756 multiplied by cosine bell functions and zero-filled once in each dimension. Spectra were
757 analysed in NMRFAM-Sparky(Lee et al., 2015) (Goddard, T.D. and Kneller, D.G, University
758 of California, San Francisco).

759 The average chemical shift differences, Δδ, were normalised using the equation
760 $\Delta\delta=[(\Delta\delta_{1H})^2+(\Delta\delta_{13C}/3.5)^2]^{0.5}$. The error values were calculated by the formula

761 $[\Delta\delta_{1H}*R_{1H}+\Delta\delta_{13C}*R_{13C}/(3.5)^2]/\Delta\delta$, where R_{1H} and R_{13C} are the digital resolutions in ppm in
762 the ^{1}H and ^{13}C dimensions respectively (Kofuku et al., 2012).
763
764 **Saturation and Competition binding assays**
765 1 nmol purified full-length α_{1A}-AR variant (mCherry attached) was resuspended in 10 mL
766 assay buffer (20 mM HEPES, pH 7.5, 100 mM NaCl, 0.02% DDM) and immobilized onto
767 200 µL of Dynabeads (Streptavidin T1) for 30 min at 4 °C. 100 µL of the suspension
768 containing beads with immobilized receptor was aliquoted to a 96-DeepWell plate from
769 which the beads transferred to another 96-DeepWell plate containing 100 µL ligand solution
770 using a KingFisher Flex magnetic particle processor. For saturation binding, immobilized
771 receptors in each well were incubated with 100 µL assay buffer containing increased
772 concentration (0, 3.125, 6.25, 12.5, 25, 50, 100, 200 nM) of QAPB (Quinazoline Piperazine
773 Bodipy) for 2 h at 22 °C. Nonspecific binding was determined by repeating the experiment
774 in the presence of 10 µM of prazosin. For competition binding, immobilized receptors were
775 incubated with 100 µL of assay buffer containing 10 nM QAPB with the addition of ligands
776 at various concentrations, as shown in the Supplementary Figures 5 and 8, for 2 h at 22 °C.
777 Immobilised receptors were subsequently washed with 200 µL of assay buffer and
778 resuspended in 100 µL assay buffer. 90 µL of the final beads solution was transferred to a 96-
779 well Greiner Bio-One nonbinding black plate. Fluorescence of bound QAPB was measured
780 using a POLARstar OMEGA plate reader (BMG Labtech, Ortenburg, Germany) and
781 normalised to mCherry fluorescence which was detected simultaneously. Data represent the
782 mean ± standard deviation (SD) of three independent biological replicate experiments each
783 performed in duplicate technical measurements. To compare ligand binding affinities at α_{1A}-
784 AR-A4 (L312F) and α_{1A}-AR-A4-active of to α_{1A}-AR-A4, raw data from our previously

785 published paper (Yong et al., 2018), were reanalysed and presented in Supplementary Table
786 1.
787
788 **Thermostability assay**
789 1 nM purified full-length α_{1A}-AR-A4 or α_{1A}-AR-A4-active (mCherry attached) was prepared
790 in base buffer (20 mM HEPES, 100 mM NaCl, 0.1% DDM). To measure thermostability of
791 receptors in the apo-state, 100 µL of receptor solution was aliquoted into 24 wells of a 96-
792 well PCR plate. 10 of the 12 duplicates were heated in gradient temperatures for 30 min and
793 the two remaining duplicates were left at 4 °C for normalisation. After thermo-treatment, the
794 receptors were transferred to a KingFisher 96-DeepWell plate containing 2 µL paramagnetic
795 Dynabeads per well (streptavidin T1, ThermoFisher Scientific). The following few steps were
796 automatically performed by using a KingFisher 96 magnetic particle processor. The receptor
797 was firstly incubated with magnetic beads for 30 min at 4 °C. Then, magnetic beads were
798 transferred to another 96-DeepWell plate containing 100 µL ligand solution (20 mM HEPES,
799 100 mM NaCl, 0.1% DDM, 100 nM QAPB). The non-specific binding was determined by
800 competing QAPB with 100 µL prazosin. After 1.5 h incubation, immobilised receptors were
801 subsequently washed with 200 µL of assay buffer and resuspended in 100 µL assay buffer. 90
802 µL of the final beads solution was transferred to a 96-well Greiner Bio-One nonbinding black
803 plate. Fluorescence of bound QAPB was measured using a POLARstar OMEGA plate reader
804 (BMG Labtech, Ortenburg, Germany) and normalised to mCherry fluorescence which was
805 detected simultaneously. To measure the thermostability of α_{1A}-AR variants in the presence
806 of ligand, receptors were preincubated with 100 nM QAPB for 1 h on ice prior to be heated at
807 varying temperatures. The remaining steps were carried out as described for apo state
808 thermostability assay. Data represent the mean ± SD of three independent biological replicate
809 experiments each performed in duplicate technical replicate measurements.

IP_1 assay

Gαq/11 signalling assays were carried out using the IP-One HTRF® Assay Kit (Cisbio Bioassays, France) measuring inositol phosphate (IP_1) using the manufacturer's protocol. COS-7 cells were seeded at 25,000 cells per well in a 96-well plate and incubated overnight at 37 °C and 5% CO_2 in Dulbecco's modified Eagle medium (DMEM) (Gibco, Gaithersburg, USA) supplemented with 10% FBS (Scientifix Life, Melbourne, Australia), 1% L-Glutamine (Gibco) and 1% penicillin/streptomycin (Gibco). Cells were transfected with pcDNA3.1 constructs of WT or mutant α_{1A}-ARs using Lipofectamine 2000 (Invitrogen, Carlsbad, USA) at 0.25 µg DNA per well. 24 h later, cells were stimulated with ligands for 2 h at 37 °C in 40 µL of Stimulation Buffer, then frozen at -80 °C. 14 µL of thawed sample were transferred to a white HTRF® 384-well Optiplate (PerkinElmer, Waltham, USA), incubated with development reagents in the dark for 1 h with shaking, and analysed by time-resolved fluorescence using a POLARstar OMEGA plate reader (BMG Labtech, Ortenburg, Germany). Data were analysed against the kit's standard curve. Data represent mean ± SD of three independent biological replicate experiments each performed in triplicate technical replicate measurements, unless otherwise stated in the figure legends.

NanoBiT G Protein Activity Assay

COS-7 cells grown in 10% fetal bovine serum (FBS), 1% L-Glutamine, 1% penicillin/streptomycin DMEM media were seeded at 250,000 cells per well on a six-well plate. Cells were then transiently co-transfected in the six-well plate, with 0.1 µg $G\alpha_q$-LgBiT (GNAQ-11S) DNA, 0.5 µg Gβ-untagged (GNB1) DNA, 0.5 µg Gγ-SmBiT (114-GnG_2) DNA, 0.2 µg Guanine Release Factor (RIC8A) DNA and 0.5 µg α_{1A}-AR (or respective AR mutants) DNA using Lipofectamine 2000 transfection reagent as per the manufacturer's

instructions. The next day the cells were resuspended in Phenol-Red-free (PRF) DMEM media containing 10% FBS, 1% L-Glutamine, 1% penicillin/streptomycin, 25 mM HEPES and seeded at 50,000 cells per well to a white 96-well plate and incubated overnight. On the day of the assay, plates were pre-incubated with 10 µM Furimazine for 1 hour. Following incubation, raw luminescence counts in each well were measured every 12 sec over the course of the assay using a POLARstar Omega plate reader (BMG Labtech). Cells were treated with either vehicle or a saturating concentration of each ligand (50 nM for A-61603 and 100 nM for antagonists). Luminescence counts were plotted against time, with the final pre-incubation reading assigned as the zero-time point (time of vehicle/ligand addition). A baseline correction was then performed by subtracting the luminescence counts in the vehicle-treated samples from the ligand-treated samples which resulted in a time-course plot of ligand-induced luminescence counts. Initial raw luminescence counts were used as a readout of G protein expression levels. Data represent the mean ± standard error (SEM) of three independent biological replicate experiments each performed in triplicate technical replicate measurements, unless otherwise stated in the figure legends.

Intracellular Ca^{2+} Mobilization Assays

COS-7 cells were seeded in 10 cm culture dishes at $3x10^6$ cells per dish and allowed to grow overnight at 37 °C, 5% CO_2 in Dulbecco's modified Eagle medium (DMEM) supplemented with 10% FBS, 1% L-Glutamine and 1% penicillin/streptomycin (Life Technologies, California, USA). The next day the cells were transfected with 30 µg of receptor DNA construct (pcDNA3.1 expression vector containing WT or mutant α_{1A}-ARs) using 60 µl of Lipofectamine 2000 (Invitrogen) transfecting reagent per dish. The following day, cells were transferred to 96-well culture plates ($5x10^4$ cells per well) and allowed to grow overnight. On the day of the experiment cells were washed twice with Ca^{2+} assay buffer [150 mM NaCl, 2.6

mM KCl, 1.2 mM $MgCl_2$, 10 mM D-glucose, 10 mM HEPES, 2.2 mM $CaCl_2$, 0.5% (w/v) BSA, and 4 mM probenecid, pH 7.4] and incubated in Ca^{2+} assay buffer containing 1 mM Fluo-4-AM for 1 h in the dark at 37 °C and 5% CO_2. After two washes with Ca^{2+} assay buffer, fluorescence was measured for 1.5 min upon the addition of ligands in a Flexstation 3 (Molecular Devices, Sunnyvale, CA) using an excitation wavelength of 485 nm and emission wavelength of 520 nm. Data were normalized to the peak response elicited by 3 μM Ionomycin (Life Technologies). Data represent the mean ± SD of three independent biological replicate experiments each performed in triplicate technical replicate measurements, unless otherwise stated in the figure legends.

Homology Modelling

Homology models of inactive- and active-state α_{1A}-AR were built with I-TASSER (Zhang et al., 2015) using crystal structures of β_2-AR as the templates. For inactive state models, the structure of β_2-AR bound to the antagonist carazolol and the inactive-state stabilizing nanobody, Nb60 (PDB ID: 5JQH) (Staus et al., 2016) was used as a template. For the active state models, the crystal structure of a β_2-AR-Gs protein complex bound to the agonist BI-167107 (PDB ID: 3SN6) (Rasmussen et al., 2011) was used as a template. The N- and C-terminal regions as well as the ICL3 regions, which have no sequence similarity to the template, were deleted from the model. Energy minimisation was performed using Minimize tool in Maestro version 11.7.012 (Schrödinger, Inc.) under OPLS 2005 (Siu et al., 2012) forcefield.

References

Ahuja, S., and Smith, S.O. (2009). Multiple switches in G protein-coupled receptor activation. Trends Pharmacol Sci *30*, 494-502.

Akinaga, J., Garcia-Sainz, J.A., and Pupo, A.S. (2019). Updates in the Function and Regulation of alpha1 -Adrenoceptors. Br J Pharmacol.

Bokoch, M.P., Zou, Y., Rasmussen, S.G., Liu, C.W., Nygaard, R., Rosenbaum, D.M., Fung, J.J., Choi, H.J., Thian, F.S., Kobilka, T.S., Puglisi, J.D., Weis, W.I., Pardo, L., Prosser, R.S., Mueller, L., and Kobilka, B.K. (2010). Ligand-specific regulation of the extracellular surface of a G-protein-coupled receptor. Nature *463*, 108-112.

Bumbak, F., Bathgate, R.A.D., Scott, D.J., and Gooley, P.R. (2019). Expression and Purification of a Functional E. coli (13)CH3-Methionine-Labeled Thermostable Neurotensin Receptor 1 Variant for Solution NMR Studies. Methods Mol Biol *1947*, 31-55.

Bumbak, F., Keen, A.C., Gunn, N.J., Gooley, P.R., Bathgate, R.A.D., and Scott, D.J. (2018). Optimization and (13)CH3 methionine labeling of a signaling competent neurotensin receptor 1 variant for NMR studies. Biochim Biophys Acta *1860*, 1372-1383.

Butterfoss, G., DeRose, E., Gabel, S., Perera, L., Krahn, J., Mueller, G., Zheng, X., and London, R. (2010). Conformational dependence of 13C shielding and coupling constants for methionine methyl groups. Journal of biomolecular NMR *48*, 31-47.

Carpenter, B., and Tate, C.G. (2017). Active state structures of G protein-coupled receptors highlight the similarities and differences in the G protein and arrestin coupling interfaces. Curr Opin Struct Biol *45*, 124-132.

Casiraghi, M., Damian, M., Lescop, E., Point, E., Moncoq, K., Morellet, N., Levy, D., Marie, J., Guittet, E., Baneres, J.L., and Catoire, L.J. (2016). Functional Modulation of a G Protein-Coupled Receptor Conformational Landscape in a Lipid Bilayer. J Am Chem Soc *138*, 11170-11175.

Clark, L.D., Dikiy, I., Chapman, K., Rodstrom, K.E., Aramini, J., LeVine, M.V., Khelashvili, G., Rasmussen, S.G., Gardner, K.H., and Rosenbaum, D.M. (2017). Ligand modulation of sidechain dynamics in a wild-type human GPCR. Elife *6*.

Cotecchia, S., Schwinn, D.A., Randall, R.R., Lefkowitz, R.J., Caron, M.G., and Kobilka, B.K. (1988). Molecular cloning and expression of the cDNA for the hamster alpha 1-adrenergic receptor. Proceedings of the National Academy of Sciences of the United States of America *85*, 7159-7163.

Delaglio, F., Grzesiek, S., Vuister, G.W., Zhu, G., Pfeifer, J., and Bax, A. (1995). NMRPipe: a multidimensional spectral processing system based on UNIX pipes. J Biomol NMR *6*, 277-293.

Deupi, X., and Standfuss, J. (2011). Structural insights into agonist-induced activation of G-protein-coupled receptors. Curr Opin Struct Biol *21*, 541-551.

Dror, R.O., Arlow, D.H., Maragakis, P., Mildorf, T.J., Pan, A.C., Xu, H., Borhani, D.W., and Shaw, D.E. (2011). Activation mechanism of the beta2-adrenergic receptor. Proc Natl Acad Sci U S A *108*, 18684-18689.

Eddy, M.T., Didenko, T., Stevens, R.C., and Wuthrich, K. (2016). beta2-Adrenergic Receptor Conformational Response to Fusion Protein in the Third Intracellular Loop. Structure *24*, 2190-2197.

Eddy, M.T., Lee, M.Y., Gao, Z.G., White, K.L., Didenko, T., Horst, R., Audet, M., Stanczak, P., McClary, K.M., Han, G.W., Jacobson, K.A., Stevens, R.C., and Wuthrich, K. (2018). Allosteric Coupling of Drug Binding and Intracellular Signaling in the A2A Adenosine Receptor. Cell *172*, 68-80 e12.

Garcia-Nafria, J., and Tate, C.G. (2019). Cryo-EM structures of GPCRs coupled to Gs, Gi and Go. Mol Cell Endocrinol *488*, 1-13.

Horst, R., Liu, J., Stevens, R., and Wüthrich, K. (2013). β2-Adrenergic Receptor Activation by Agonists Studied with19F NMR Spectroscopy. Angewandte Chemie *125*, 10962-10965.

Hwa, J., Graham, R.M., and Perez, D.M. (1995). Identification of critical determinants of alpha 1-adrenergic receptor subtype selective agonist binding. J Biol Chem *270*, 23189-23195.

Inoue, A., Raimondi, F., Kadji, F.M.N., Singh, G., Kishi, T., Uwamizu, A., Ono, Y., Shinjo, Y., Ishida, S., Arang, N., Kawakami, K., Gutkind, J.S., Aoki, J., and Russell, R.B. (2019). Illuminating G-Protein-Coupling Selectivity of GPCRs. Cell.

Isberg, V., de Graaf, C., Bortolato, A., Cherezov, V., Katritch, V., Marshall, F., Mordalski, S., Pin, J.-P., Stevens, R., Vriend, G., and Gloriam, D. (2015). Generic GPCR residue numbers – aligning topology maps while minding the gaps. Trends in pharmacological sciences (Regular ed, Print) *36*, 22-31.

Isogai, S., Deupi, X., Opitz, C., Heydenreich, F.M., Tsai, C.J., Brueckner, F., Schertler, G.F., Veprintsev, D.B., and Grzesiek, S. (2016). Backbone NMR reveals allosteric signal transduction networks in the beta1-adrenergic receptor. Nature *530*, 237-241.

Kofuku, Y., Ueda, T., Okude, J., Shiraishi, Y., Kondo, K., Maeda, M., Tsujishita, H., and Shimada, I. (2012). Efficacy of the beta(2)-adrenergic receptor is determined by conformational equilibrium in the transmembrane region. Nat Commun *3*, 1045.

Kofuku, Y., Ueda, T., Okude, J., Shiraishi, Y., Kondo, K., Mizumura, T., Suzuki, S., and Shimada, I. (2014). Functional dynamics of deuterated beta2 -adrenergic receptor in lipid bilayers revealed by NMR spectroscopy. Angew Chem Int Ed Engl *53*, 13376-13379.

Latorraca, N.R., Venkatakrishnan, A.J., and Dror, R.O. (2017). GPCR Dynamics: Structures in Motion. Chem Rev *117*, 139-155.

Lee, W., Tonelli, M., and Markley, J.L. (2015). NMRFAM-SPARKY: enhanced software for biomolecular NMR spectroscopy. Bioinformatics *31*, 1325-1327.

Liu, J.J., Horst, R, et al. (2012). biased signaling pathways in beta2-AR characterized by 19F-NMR Science.

Manglik, A., Kim, T.H., Masureel, M., Altenbach, C., Yang, Z., Hilger, D., Lerch, M.T., Kobilka, T.S., Thian, F.S., Hubbell, W.L., Prosser, R.S., and Kobilka, B.K. (2015). Structural Insights into the Dynamic Process of beta2-Adrenergic Receptor Signaling. Cell *161*, 1101-1111.

Manglik, A., and Kruse, A.C. (2017). Structural Basis for G Protein-Coupled Receptor Activation. Biochemistry *56*, 5628-5634.

Nygaard, R., Zou, Y., Dror, R.O., Mildorf, T.J., Arlow, D.H., Manglik, A., Pan, A.C., Liu, C.W., Fung, J.J., Bokoch, M.P., Thian, F.S., Kobilka, T.S., Shaw, D.E., Mueller, L., Prosser, R.S., and Kobilka, B.K. (2013). The dynamic process of beta(2)-adrenergic receptor activation. Cell *152*, 532-542.

Okude, J., Ueda, T., Kofuku, Y., Sato, M., Nobuyama, N., Kondo, K., Shiraishi, Y., Mizumura, T., Onishi, K., Natsume, M., Maeda, M., Tsujishita, H., Kuranaga, T., Inoue, M., and Shimada, I. (2015). Identification of a Conformational Equilibrium That Determines the Efficacy and Functional Selectivity of the mu-Opioid Receptor. Angew Chem Int Ed Engl *54*, 15771-15776.

Perez, D., and Doze, V. (2011). Cardiac and neuroprotection regulated by alpha(1)-adrenergic receptor subtypes. Journal of receptor and signal transduction research *31*, 98-110.

Rasmussen, S.G., DeVree, B.T., Zou, Y., Kruse, A.C., Chung, K.Y., Kobilka, T.S., Thian, F.S., Chae, P.S., Pardon, E., Calinski, D., Mathiesen, J.M., Shah, S.T., Lyons, J.A., Caffrey, M., Gellman, S.H., Steyaert, J., Skiniotis, G., Weis, W.I., Sunahara, R.K., and Kobilka, B.K. (2011). Crystal structure of the beta2 adrenergic receptor-Gs protein complex. Nature *477*, 549-555.

Schanda, P., Kupce, E., and Brutscher, B. (2005). SOFAST-HMQC experiments for recording two-dimensional heteronuclear correlation spectra of proteins within a few seconds. J Biomol NMR *33*, 199-211.

Scott, D.J., Gunn, N.J., Yong, K.J., Wimmer, V.C., Veldhuis, N.A., Challis, L.M., Haidar, M., Petrou, S., Bathgate, R.A.D., and Griffin, M.D.W. (2018). A Novel Ultra-Stable, Monomeric Green Fluorescent Protein For Direct Volumetric Imaging of Whole Organs Using CLARITY. Sci Rep *8*, 667.

Scott, D.J., and Pluckthun, A. (2013). Direct molecular evolution of detergent-stable G protein-coupled receptors using polymer encapsulated cells. J Mol Biol *425*, 662-677.

Shimada, I., Ueda, T., Kofuku, Y., Eddy, M.T., and Wuthrich, K. (2018). GPCR drug discovery: integrating solution NMR data with crystal and cryo-EM structures. Nat Rev Drug Discov.

Siu, S.W., Pluhackova, K., and Bockmann, R.A. (2012). Optimization of the OPLS-AA Force Field for Long Hydrocarbons. J Chem Theory Comput *8*, 1459-1470.

983 Solt, A.S., Bostock, M.J., Shrestha, B., Kumar, P., Warne, T., Tate, C.G., and Nietlispach, D. (2017).
984 Insight into partial agonism by observing multiple equilibria for ligand-bound and Gs-mimetic
985 nanobody-bound beta1-adrenergic receptor. Nat Commun *8*, 1795.
986 Sounier, R., Mas, C., Steyaert, J., Laeremans, T., Manglik, A., Huang, W., Kobilka, B.K., Demene, H.,
987 and Granier, S. (2015). Propagation of conformational changes during mu-opioid receptor activation.
988 Nature *524*, 375-378.
989 Staus, D.P., Strachan, R.T., Manglik, A., Pani, B., Kahsai, A.W., Kim, T.H., Wingler, L.M., Ahn, S.,
990 Chatterjee, A., Masoudi, A., Kruse, A.C., Pardon, E., Steyaert, J., Weis, W.I., Prosser, R.S., Kobilka,
991 B.K., Costa, T., and Lefkowitz, R.J. (2016). Allosteric nanobodies reveal the dynamic range and
992 diverse mechanisms of G-protein-coupled receptor activation. Nature *535*, 448-452.
993 Trzaskowski, B., Latek, D., Yuan, S., Ghoshdastider, U., Debinski, A., and Filipek, S. (2012). Action of
994 molecular switches in GPCRs--theoretical and experimental studies. Curr Med Chem *19*, 1090-1109.
995 Xu, J., Hu, Y., Kaindl, J., Risel, P., Hubner, H., Maeda, S., Niu, X., Li, H., Gmeiner, P., Jin, C., and
996 Kobilka, B.K. (2019). Conformational Complexity and Dynamics in a Muscarinic Receptor Revealed by
997 NMR Spectroscopy. Mol Cell.
998 Ye, L., Neale, C., Sljoka, A., Lyda, B., Pichugin, D., Tsuchimura, N., Larda, S.T., Pomes, R., Garcia, A.E.,
999 Ernst, O.P., Sunahara, R.K., and Prosser, R.S. (2018). Mechanistic insights into allosteric regulation of
1000 the A2A adenosine G protein-coupled receptor by physiological cations. Nat Commun *9*, 1372.
1001 Ye, L., Van Eps, N., Zimmer, M., Ernst, O.P., and Prosser, R.S. (2016). Activation of the A2A adenosine
1002 G-protein-coupled receptor by conformational selection. Nature *533*, 265-268.
1003 Yong, K.J., Vaid, T.M., Shilling, P.J., Wu, F.J., Williams, L.M., Deluigi, M., Pluckthun, A., Bathgate,
1004 R.A.D., Gooley, P.R., and Scott, D.J. (2018). Determinants of Ligand Subtype-Selectivity at alpha1A-
1005 Adrenoceptor Revealed Using Saturation Transfer Difference (STD) NMR. ACS Chem Biol *13*, 1090-
1006 1102.
1007 Zhang, J., Yang, J., Jang, R., and Zhang, Y. (2015). GPCR-I-TASSER: A Hybrid Approach to G Protein-
1008 Coupled Receptor Structure Modeling and the Application to the Human Genome. Structure *23*,
1009 1538-1549.
1010 Zhu, J., Taniguchi, T., Takauji, R., Suzuki, F., Tanaka, T., and Muramatsu, I. (2000). Inverse agonism
1011 and neutral antagonism at a constitutively active alpha-1a adrenoceptor. British Journal of
1012 Pharmacology *131*, 546-552.

1013

1014

Supplementary Figures and Tables

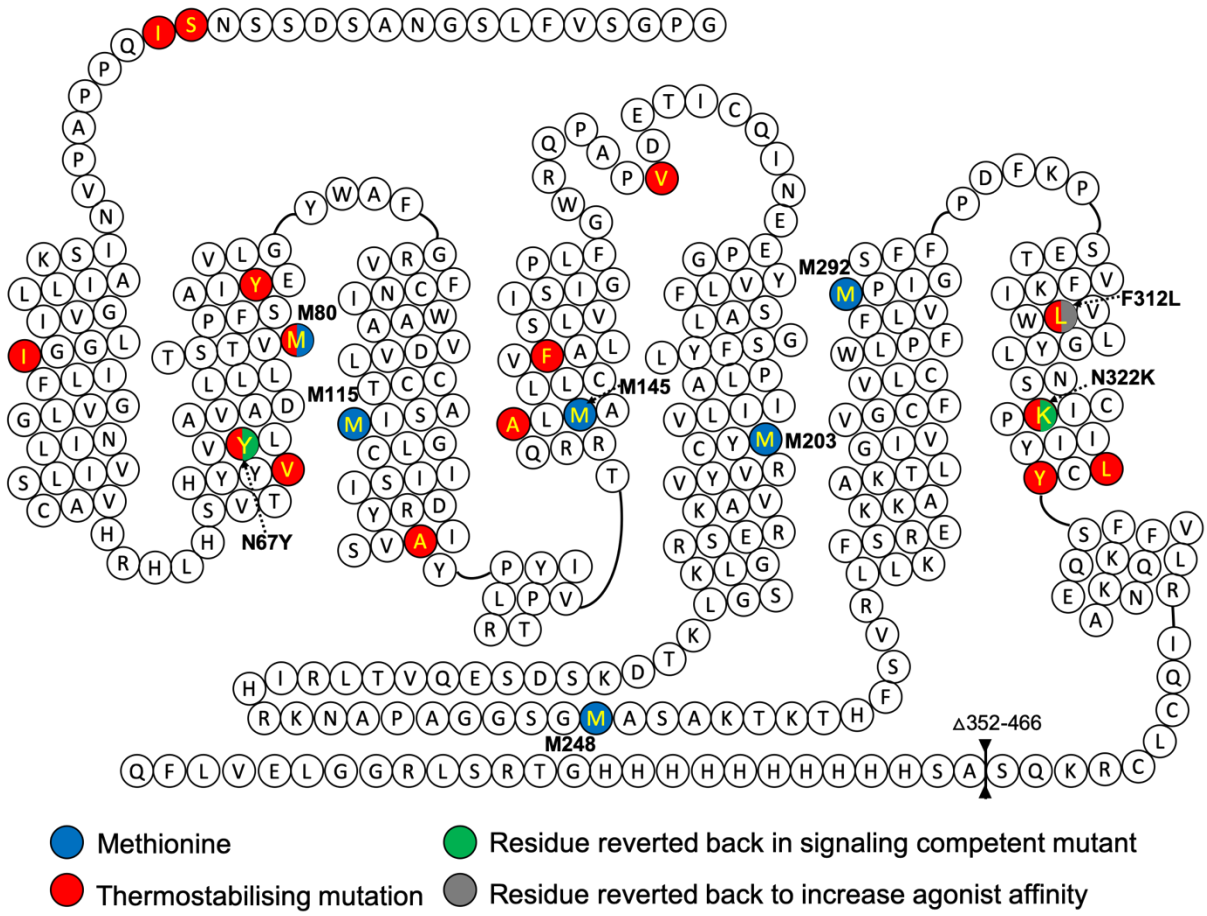

Supplementary Figure 1. Secondary structure diagram of human α_{1A}-AR-A4. Methionine residues and thermostabilisation mutations are labelled in blue and red, respectively. Two thermostabilisation mutations (N67Y, N322K) labelled in both red and green were reverted back to natural residues in making signaling competent construct α_{1A}-AR-A4-active (Y67N, K322N). Residue labelled in grey is critical for ligand binding, α_{1A}-AR-A4 (L312F) construct was made to rescue affinities of agonists tested in this study.

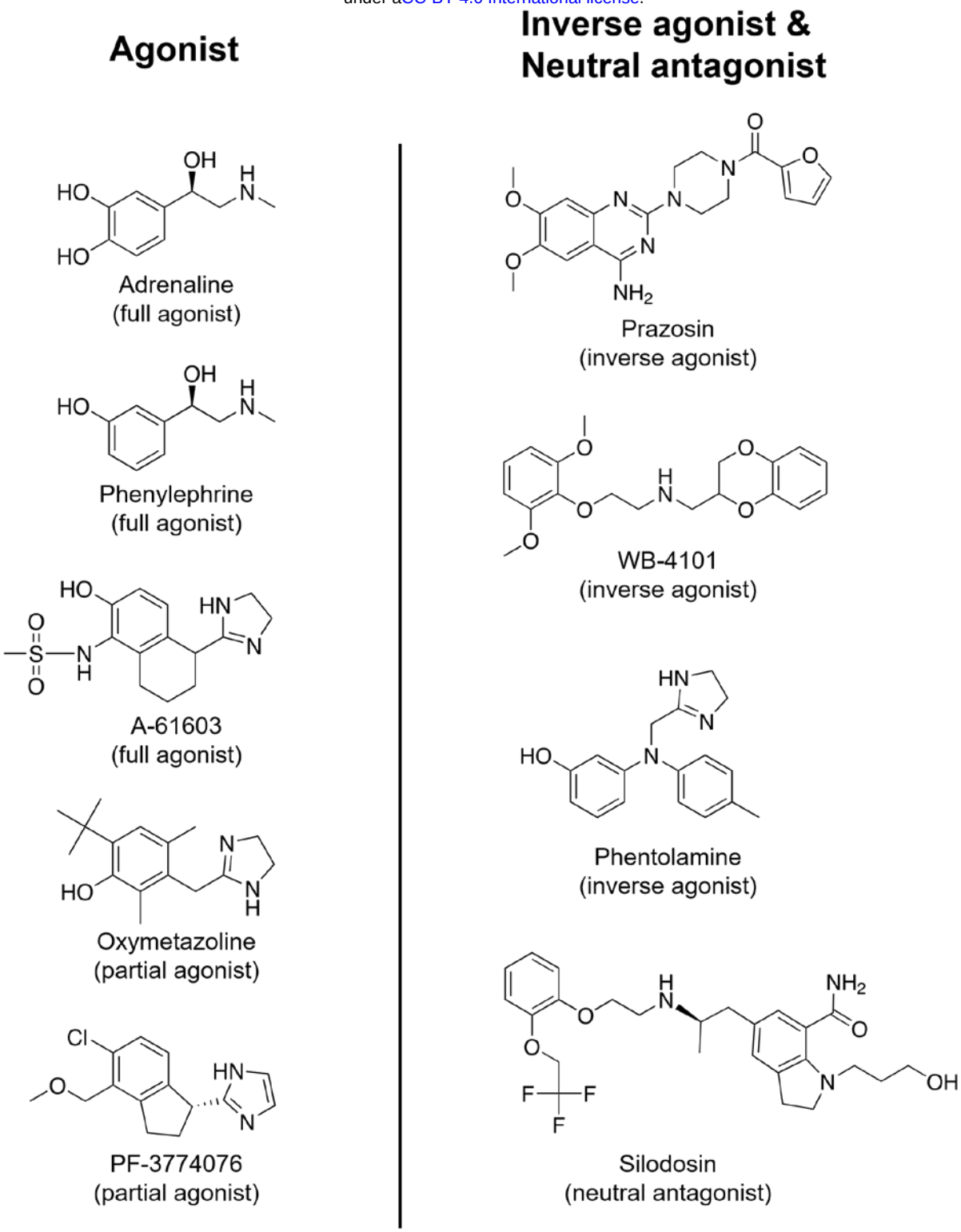

Supplementary Figure 2. Chemical structures of ligands used in this study.

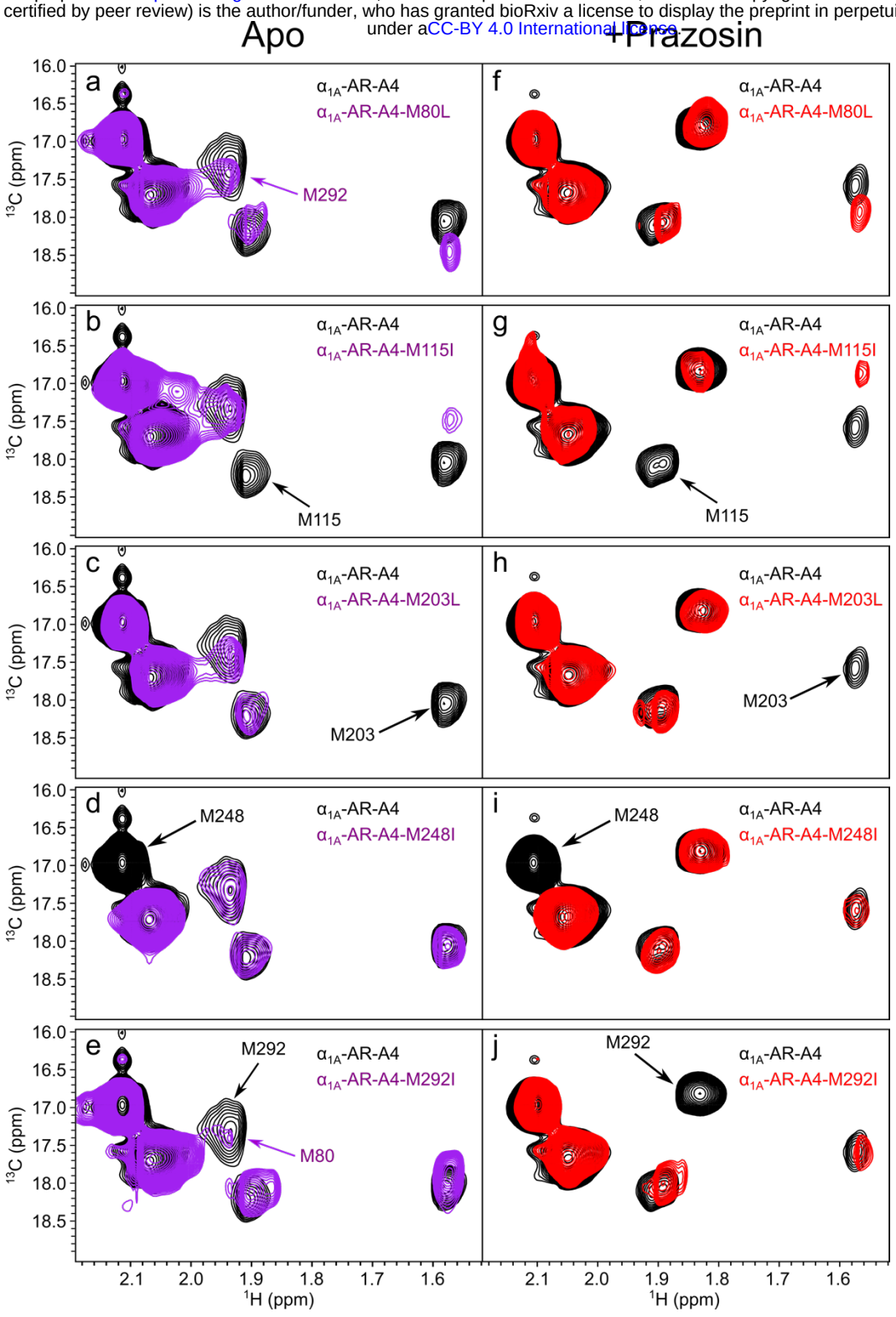

Supplementary Figure 3. Assignment of ^{13}C methyl labelled methionine residues in α_{1A}-AR-A4. Five methionine residues in α_{1A}-AR-A4 were individually mutated to either Leucine or Isoleucine, M80L (a,f); M115I (b,g); M203L (c,h); M248I (d,i); M292I (e,j). The ^{1}H-^{13}C SOFAST HMQC spectra of five α_{1A}-AR-A4 mutants were collected in apo state (a-e, purple) and prazosin-bound state (f-j, red). Spectra of all mutants overlay with the spectrum of α_{1A}-AR-A4 in the apo or prazosin-bound state (black).

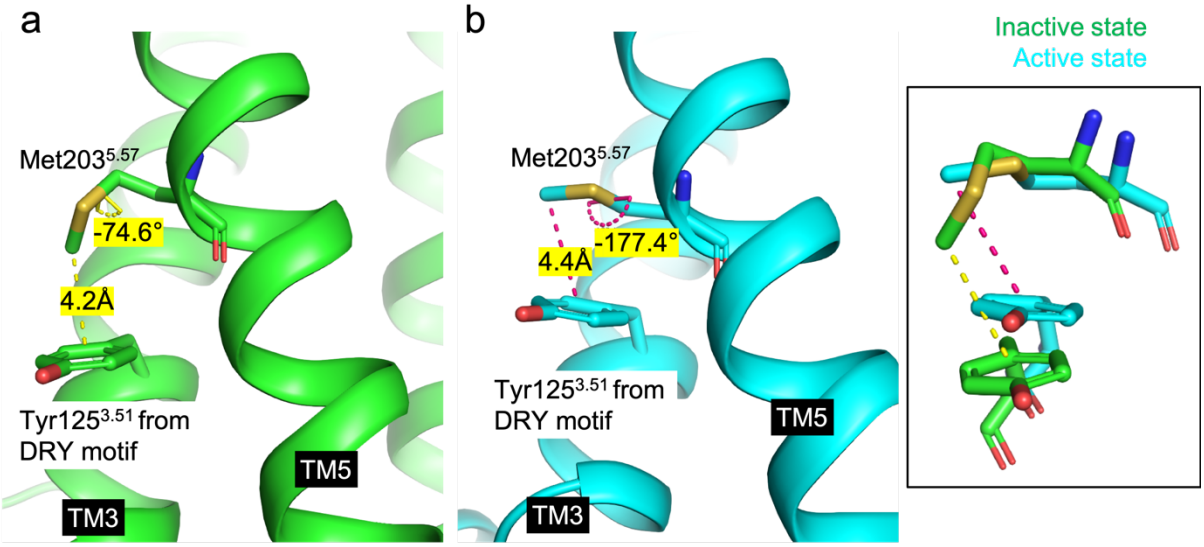

Supplementary Figure 4. The local environment of Met203$^{5.57}$ and its χ3 dihedral angle. The methyl group of Met203$^{5.57}$ sits on top of Tyr125$^{3.51}$ of the DRY motif as shown in the α_{1A}-AR-A4 homology models, and is expected to experience a ring current effect from Tyr125$^{3.51}$. (a) In the inactive state of α_{1A}-AR-A4 model (green), the distance between the methyl of Met203$^{5.57}$ and the ring of Tyr125$^{3.51}$ is 4.2Å. The χ3 dihedral angle of Met203$^{5.57}$ is -74.6º, which means the χ3 in the inactive state is averaging between gauche and trans conformers. (b) In the active state of α_{1A}-AR-A4 model (cyan), the distance between the methyl of Met203$^{5.57}$ and the ring of Tyr125$^{3.51}$ is 4.4Å. The χ3 dihedral angle of Met203$^{5.57}$ is -177.4º, which means the χ3 in the active state is in a near trans conformer.

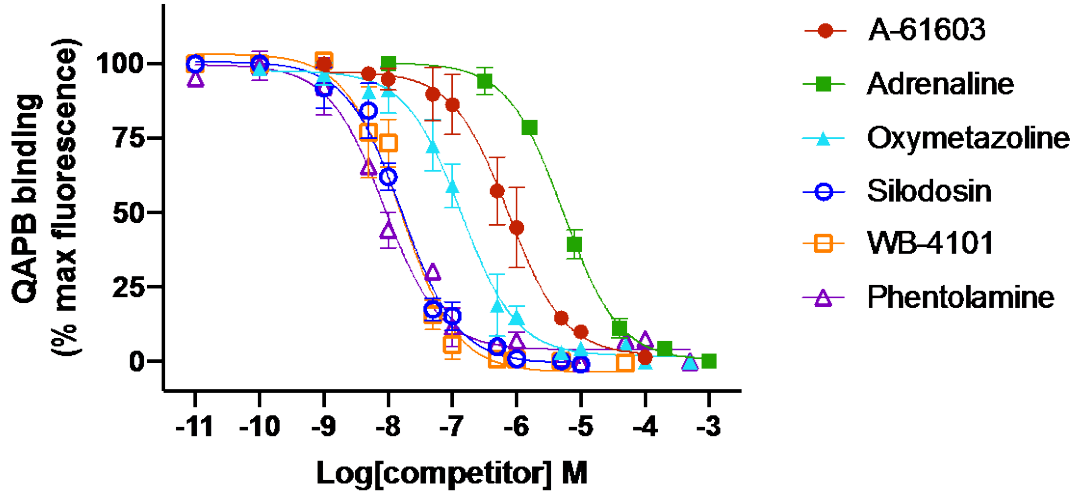

Supplementary Figure 5. Characterisation of ligand affinity to α_{1A}-AR-A4 (L312F). QAPB competition binding for 2 hours at 22 °C against purified α_{1A}-AR-A4 (L312F) with A-61603 (maroon, solid circles), adrenaline (green, solid squares), oxymetazoline (cyan, solid triangles), silodosin (blue, open circles), WB-4101 (orange, open squares) and phentolamine (purple, open triangles).

Supplementary Table 1. Measured affinities of ligands utilised in the present study.[a]

	α_{1A}-AR WT	α_{1A}-AR-A4	α_{1A}-AR-A4 (L312F)	α_{1A}-AR-A4-active
QAPB K_D (nM)	N.D	11.6 ± 2.0[1]	30.3 ± 21.2	29.2 ± 15.1
	K_i[b]	K_i	K_i	K_i
Adrenaline	3.3 ± 0.4 µM[2]	>1.0 mM[1]	2.7 ± 0.5 µM	0.4 ± 0.1 mM
Phenylephrine	6.2 ± 1.5 µM[2]	~0.6 mM[1]	41.9 ± 26.6 µM[1]	1.6 ± 0.6 mM
A-61603	~79.4 nM[3]	113.5 ± 47.2 µM[1]	0.4 ± 0.2 µM	18.4 ± 18.9 µM
Oxymetazoline	6.7 ± 0.9 nM[4]	52.8 ± 8.0 µM	65.7 ± 24.4 nM	9.7 ± 6.4 µM
PF-3774076	~83.0 nM[5]	N.D	N.D	19.4 ± 12.9 µM
Silodosin	0.036 ± 0.010 nM[4]	N.D	8.4 ± 1.9 nM	N.D
Phentolamine	2.7 ± 0.1 nM[4]	N.D	3.9 ± 2.0 nM	N.D
WB-4101	0.21 ± 0.03 nM[4]	N.D	7.6 ± 3.4 nM	N.D
Prazosin	0.17 ± 0.02 nM[4]	57.0 ± 11.8 nM[1]	7.5 ± 3.8 nM[1]	N.D

[a] Data are presented as mean K_i ± SD and mean K_D ± SD, except for the data cited from the literature which are mean K_i ± SEM and mean K_D ± SEM. Three independent biological replicate experiments (n=3) were done for all data. N.D, not determined. [b]These K_i were measured on cells overexpressed with WT human α_{1A}-AR. K_i of ligands on α_{1A}-AR-A4, α_{1A}-AR-A4 (L312F) and α_{1A}-AR-A4-active were determined with purified receptors using Kingfisher binding assay (see methods). For some ligand-receptor pairings, full displacement in competition binding assays was not observed, and thus only approximate K_i values could be estimated (indicated with ~)

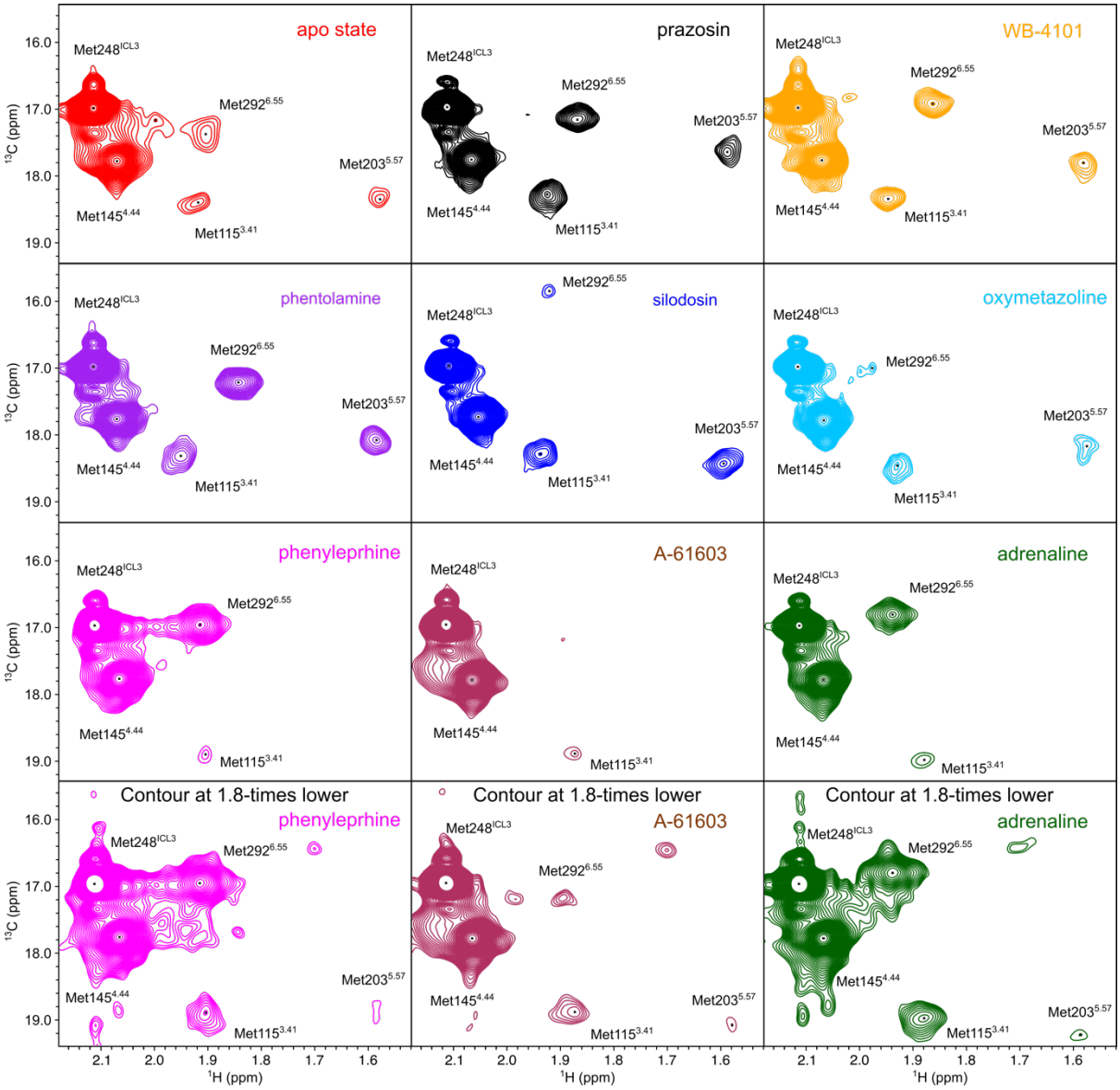

Supplementary Figure 6. ^{1}H-^{13}C SOFAST-HMQC spectra of α_{1A}-AR-A4 (L312F). Individual NMR spectrum for [$^{13}C^{\varepsilon}H_3$-Met] α_{1A}-AR-A4 (L312F) collected in the apo-state (red) and bound to prazosin (black, inverse agonist), WB-4101 (yellow, inverse agonist), phentolamine (purple, inverse agonist), silodosin (blue, neutral antagonist), oxymetazoline (cyan, partial agonist), phenylephrine (magenta, full agonist), A-61603 (maroon, full agonist), and adrenaline (green, full agonist).

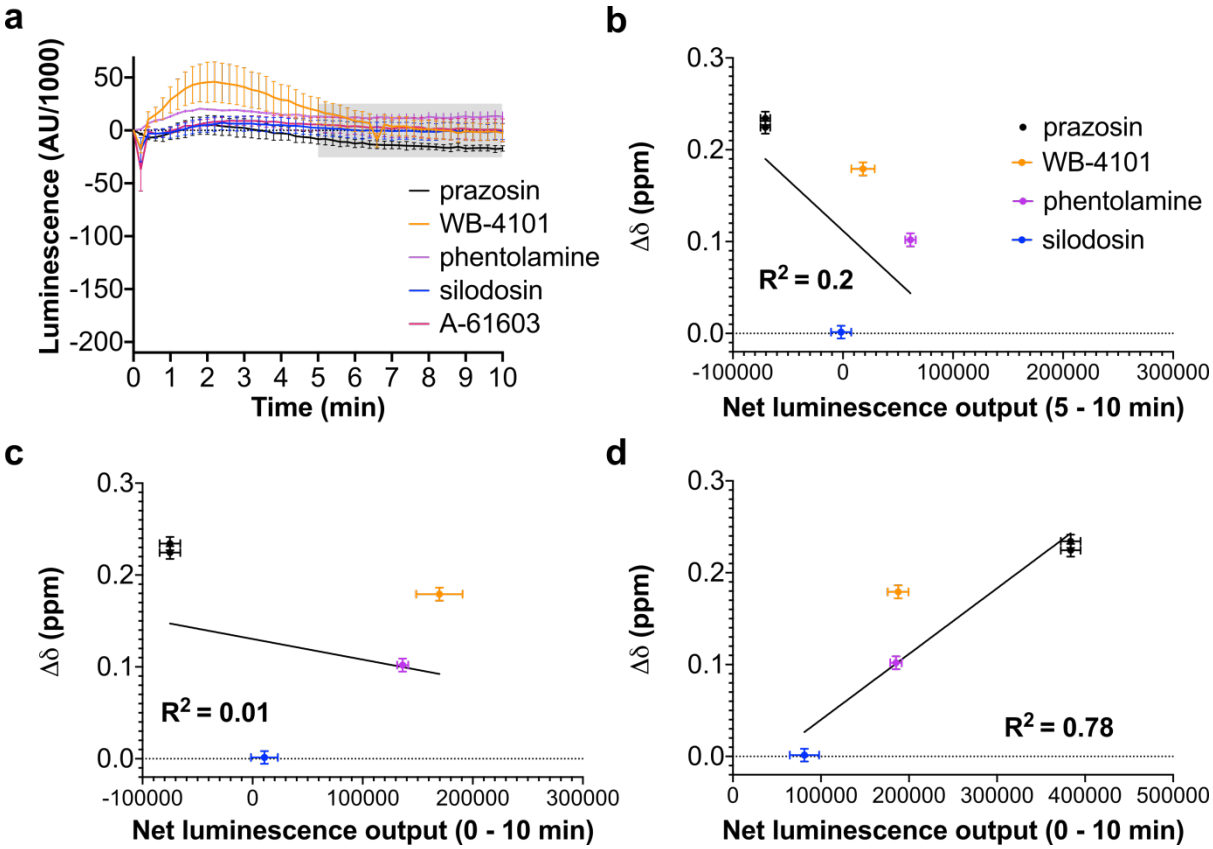

Supplementary Figure 7. **Controls for NanoBit G protein activity assay.** (a) NanoBit G protein activity assay on empty vector (pcDNA3.1/Zeo) transfected COS-7 cells treated with the same concentrations of prazosin, WB-4101, phentolamine and silodosin as in Figure 4b. The grey shaded region indicates where the area under the curve measurements were taken for (b). (b) Linear regression analysis of the average chemical shift differences (Δδ) for the $^{13}C^{\varepsilon}H_3$ of Met203 in α_{1A}-AR-A4 (L312F) and the increase in luminescence seen between 5 – 10 min after treatment in the NanoBit assay on empty vector (pcDNA3.1/Zeo) transfected COS-7 cells. A P value of 0.2663 was obtained when testing against the null hypothesis of a slope of 0 (c) Linear regression analysis of the average chemical shift differences (Δδ) for the $^{13}C^{\varepsilon}H_3$ of Met203 in α_{1A}-AR-A4 (L312F) and the increase in luminescence seen for the first 10 min after treatment in the NanoBit assay on empty vector (pcDNA3.1/Zeo) transfected COS-7 cells. Ligands are coloured as listed above and a P value of 0.6754 indicated slope not deviating significantly from 0. (d) Linear regression analysis of the average chemical shift differences (Δδ) for the $^{13}C^{\varepsilon}H_3$ of Met203 in α_{1A}-AR-A4 (L312F) and the increase in luminescence seen for the first 10 min after treatment in the NanoBit assay on COS-7 cells transfected with wild-type α_{1A}-AR (as in Figure 4b-c). A P value of 0.0071 suggested a significantly non-zero slope. Ligands are coloured as listed above. In (b), (c) and (d) Δδ are plotted for two independent titrations of prazosin and silodosin, and single experiments for WB-4101 and phentolamine. Average chemical shift differences (Δδ) were normalised using the equation $\Delta\delta=[(\Delta\delta_{1H})^2+(\Delta\delta_{13C}/3.5)^2]^{0.5}$ and errors were calculated by the formula $[\Delta\delta_{1H}*R_{1H}+\Delta\delta_{13C}*R_{13C}/(3.5)^2]/\Delta\delta$, where R_{1H} and R_{13C} are the digital resolutions in ppm in the ^{1}H and ^{13}C dimensions respectively.

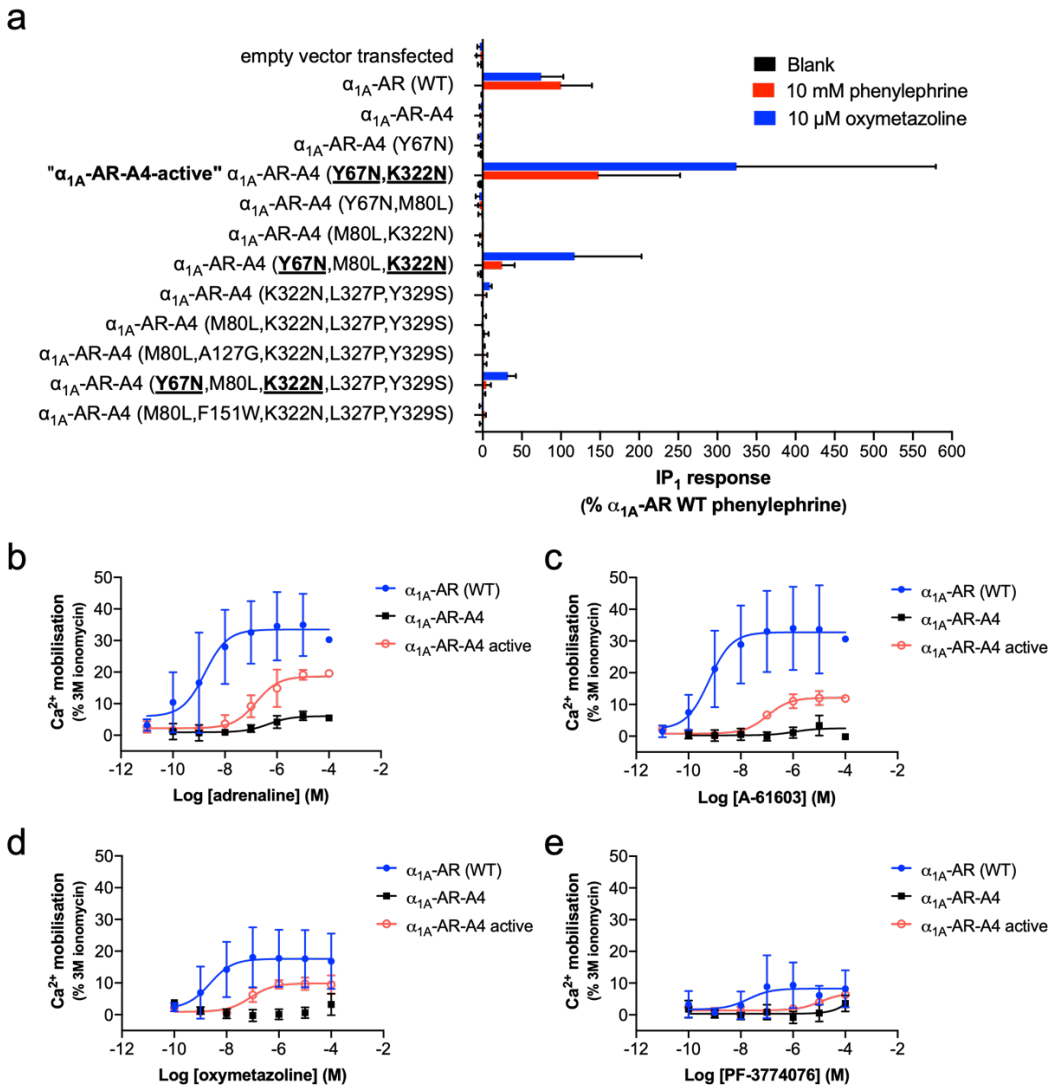

Supplementary Figure 8. Functional signalling assays performed on α_{1A}-AR-A4 active and other mutants. (a) Measurement of agonist (phenylephrine and oxymetazoline) induced accumulation of IP_1 in COS-7 cells transfected with WT α_{1A}-AR, α_{1A}-AR-A4 and mutants that were made with reverted mutations on α_{1A}-AR-A4. Y67N, M80L, A127G, F151W, K322N, L327P and Y329S are the predicted critical back mutations that were screened to recover the signaling ability of α_{1A}-AR-A4. All of α_{1A}-AR-A4 back mutants containing Y67N and K322N (highlighted with bold and underlined) displayed accumulation of IP_1 signal upon agonist activation. α_{1A}-AR-A4 (Y67N, K322N) is labelled as α_{1A}-AR-A4-active. In this screening assay some mutants were only measured in one biological replicate experiment (α_{1A}-AR-A4 (M80L,K322N,L327P,Y329S; α_{1A}-AR-A4 (K322N,L327P,Y329S); α1A-AR-A4 (Y67N,M80L,K322N); α_{1A}-AR-A4 (M80L,K322N); α_{1A}-AR-A4 (Y67N,K322N); α_{1A}-AR-A4), with the others measured in two independent biological replicate experiments, with data plotted as mean ± SD of replicate measurements. (b-e) Measurement of adrenaline (b), A-61603 (c), oxymetazoline (d) and PF-3774076 (e) induced Ca^{2+} mobilization in COS-7 cells transfected with α_{1A}-AR (blue, solid circles), α_{1A}-AR-A4 (black, solid squares) and α_{1A}-AR-A4 active (red, open circles). Data represent the mean ± SD from three independent biological replicate experiments, each measured as three technical replicates.

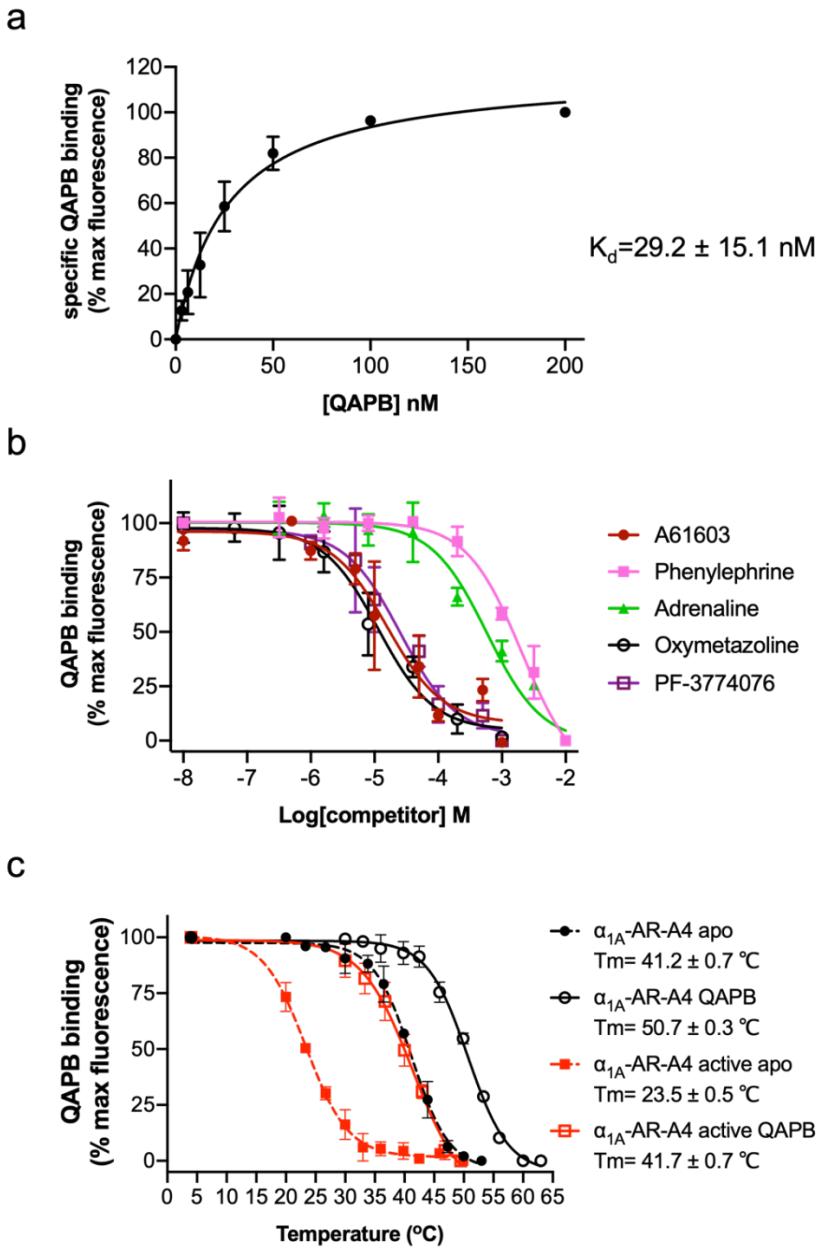

Supplementary Figure 9. Characterisation of α_{1A}-AR-A4-active. (a) Saturation binding of QAPB to purified α_{1A}-AR-A4 active. (b) QAPB competition binding for 2 hours at 22 °C against purified α_{1A}-AR-A4 active with A-61603 (maroon, solid circles), phenylephrine (pink, solid squares), adrenaline (green, solid triangles), oxymetazoline (black, open circles), PF-3774076 (purple, open squares). (c) Thermostability assay performed on α_{1A}-AR-A4 in the apo state (black solid circles and dash line), QAPB-bound state (black open circles and solid line) and α_{1A}-AR-A4-active in the apo state (red solid squares and dash line), QAPB-bound state (red open squares and solid line).

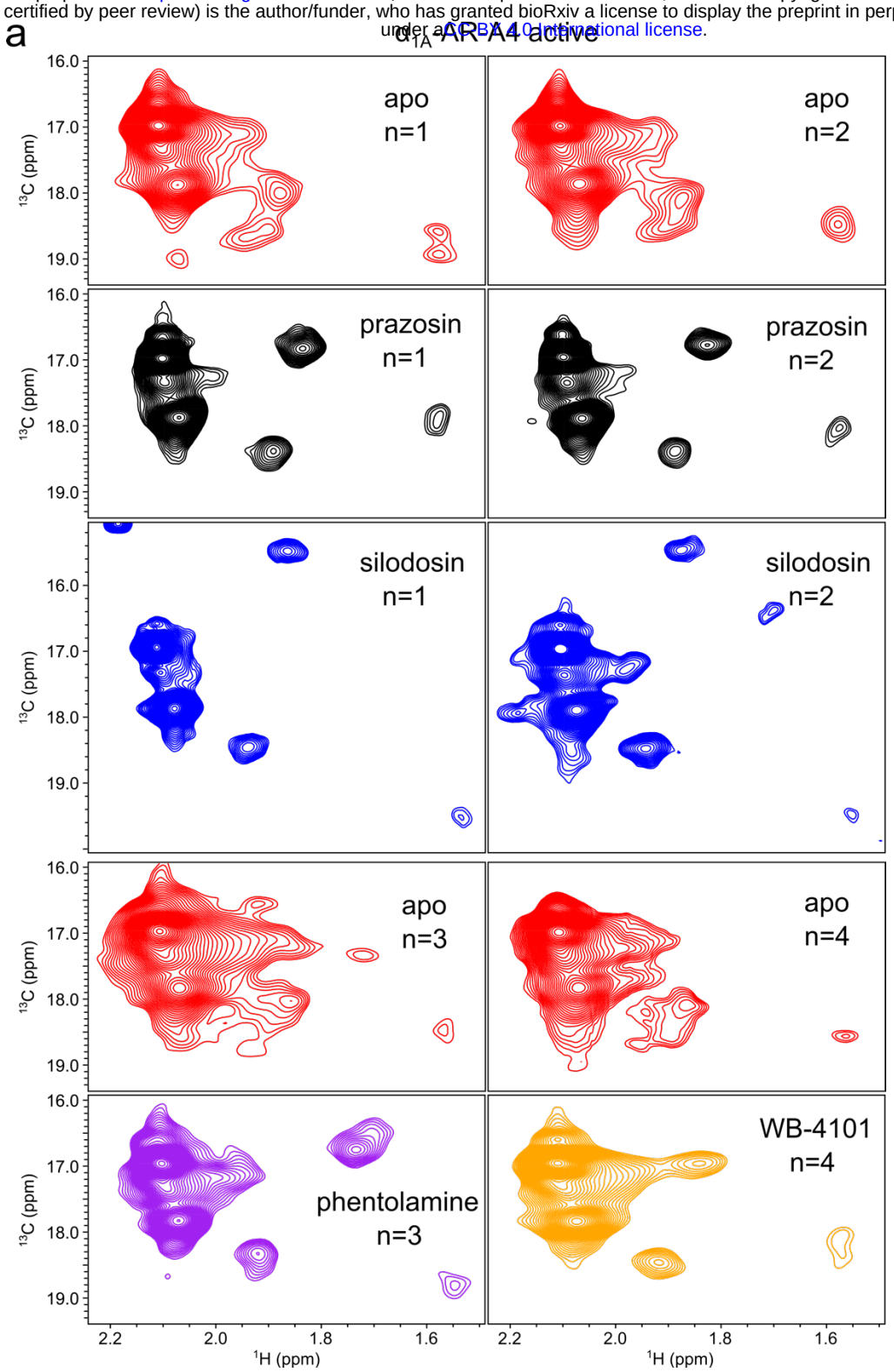

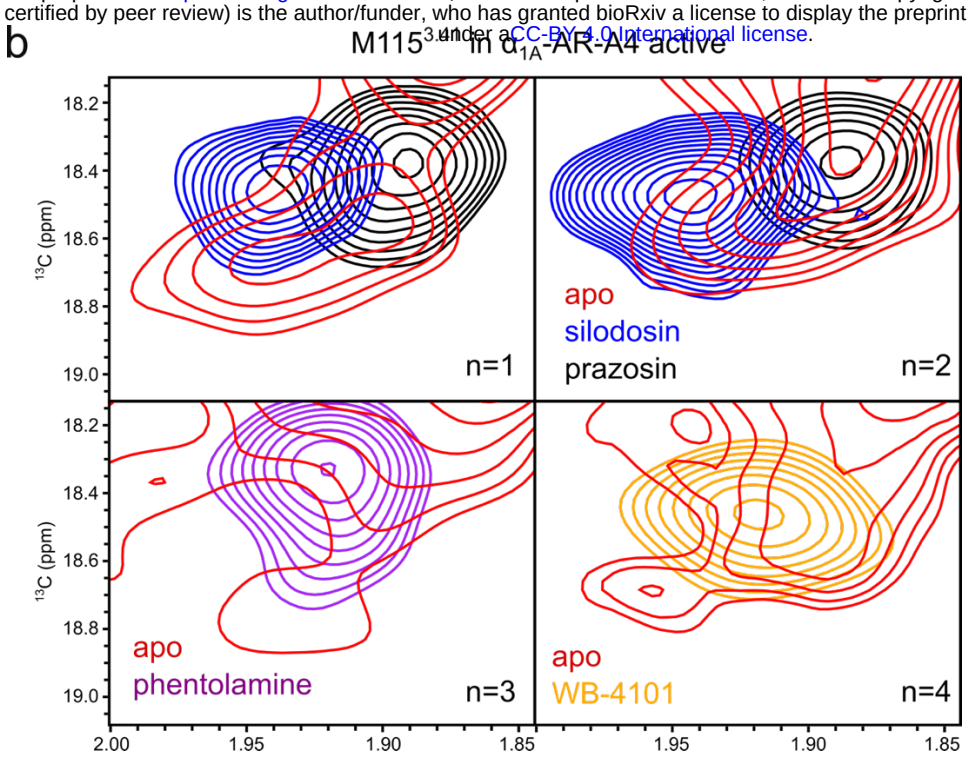

Supplementary Figure 10. **^{1}H-^{13}C SOFAST-HMQC spectra of α_{1A}-AR-A4-active.** (a) Four separate expressions and purifications of α_{1A}-AR-A4-active were conducted and data acquired for apo- (red), prazosin (black) and silodosin (blue), phentolamine (purple) and WB-4101 (orange). (b) Expansions and overlay of the region where the $^{13}C^{\varepsilon}H_3$ of Met115 resonates.

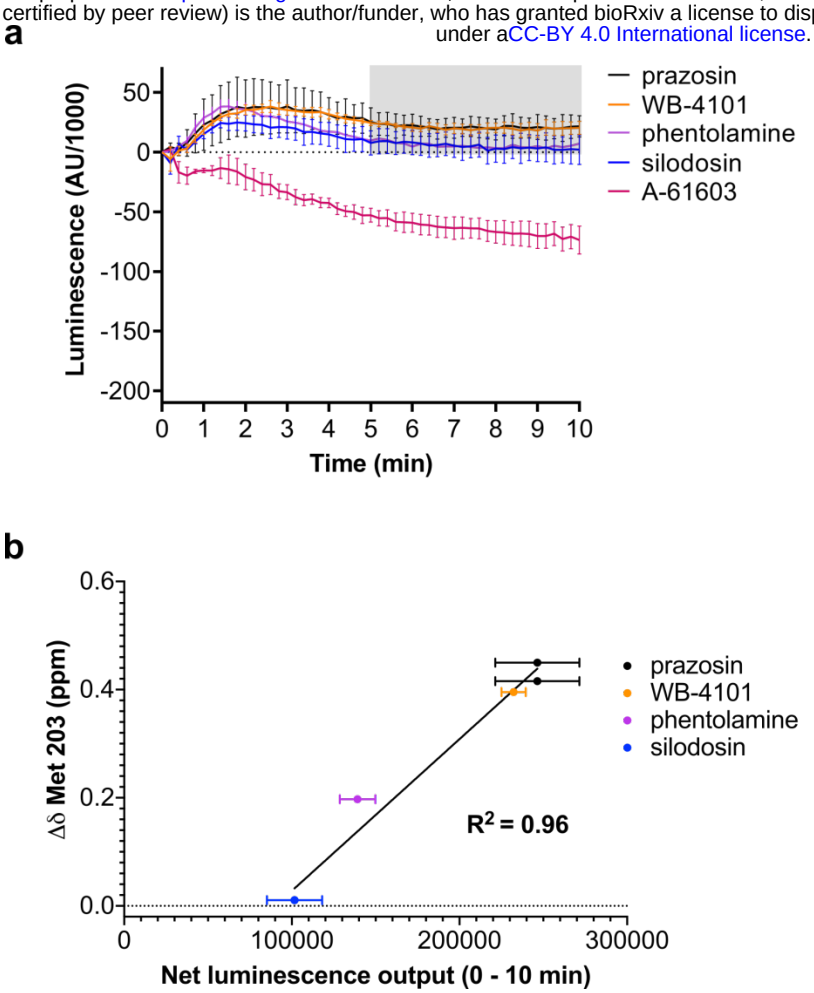

Supplementary Figure 11. **Correlation between the chemical shift position of Met203$^{5.57}$ in α_{1A}-AR-A4-active and inverse agonists efficacy.** (a) NanoBit G protein activity assay demonstrating inverse agonism of prazosin, WB-4101, phentolamine and silodosin at α_{1A}-AR-A4 active expressing COS-7 cells. The grey shaded region indicates where the area under the curve measurements were taken to make Figure 5e. (b) Linear regression analysis of the average chemical shift differences (Δδ) for the $^{13}C^{\varepsilon}H_3$ of Met203 in α_{1A}-AR-A4-active and the increase in luminescence seen over the first 10 minutes in the NanoBit assay for each antagonist. A P value of 0.0002 suggested that the slope was significantly different from zero. In (b) Δδ are plotted for two independent titrations of prazosin and silodosin, and single experiments for WB-4101 and phentolamine. Average chemical shift differences (Δδ Met 203) were normalised using the equation $\Delta\delta=[(\Delta\delta_{1H})^2+(\Delta\delta_{13C}/3.5)^2]^{0.5}$ and errors were calculated by the formula $[\Delta\delta_{1H}*R_{1H}+\Delta\delta_{13C}*R_{13C}/(3.5)^2]/\Delta\delta$, where R_{1H} and R_{13C} are the digital resolutions in ppm in the ^{1}H and ^{13}C dimensions respectively.

Reference

1. Yong, K.J. et al. Determinants of Ligand Subtype-Selectivity at alpha1A-Adrenoceptor Revealed Using Saturation Transfer Difference (STD) NMR. *ACS Chem Biol* **13**, 1090-1102 (2018).
2. Hwa, J. & Perez, D.M. The unique nature of the serine interactions for alpha 1-adrenergic receptor agonist binding and activation. *Journal of Biological Chemistry* **271**, 6322-6327 (1996).
3. Willems, E.W. et al. A61603-induced vasoconstriction in porcine carotid vasculature: involvement of a non-adrenergic mechanism. *Eur J Pharmacol* **417**, 195-201 (2001).
4. Shibata, K. et al. KMD-3213, a novel, potent, alpha 1a-adrenoceptor-selective antagonist: characterization using recombinant human alpha 1-adrenoceptors and native tissues. *Mol Pharmacol* **48**, 250-8 (1995).
5. Conlon, K. et al. Pharmacological properties of 2-((R-5-chloro-4-methoxymethylindan-1-yl)-1H-imidazole (PF-3774076), a novel and selective alpha1A-adrenergic partial agonist, in in vitro and in vivo models of urethral function. *J Pharmacol Exp Ther* **330**, 892-901 (2009).